

ANO
2018

SIMON MARCEL BRUNNQUELL | DEVELOPMENT OF CARBON ELECTRODES FOR
THE MEASUREMENT OF SKIN IMPEDANCE



UDESC

UNIVERSIDADE DO ESTADO DE SANTA CATARINA – UDESC
CENTRO DE CIÊNCIAS TECNOLÓGICAS
PROGRAMA DE PÓS GRADUAÇÃO EM ENGENHARIA ELÉTRICA

The aim of this work was to develop two impedance probes whose electrodes were based on carbon and to test their usability for the measurement of skin impedance. Knowing the passive electrical properties is of importance e.g. for dosimetry purposes. Broadband frequency sweeps were conducted on the palm of the left hand of the author in a dry and a wet state. This work contributes data of passive electric properties of palmar skin which showed considerable differences to skin electric properties in other body regions.

Orientador: Pedro Bertemes-Filho

Coorientadora: Carla Dalmolin

Joinville, 2018

DISSERTAÇÃO DE MESTRADO

**DEVELOPMENT OF CARBON
ELECTRODES FOR THE
MEASUREMENT OF SKIN
IMPEDANCE**

Simon Marcel Brunnquell

JOINVILLE, 2018

Development of Carbon Electrodes for the Measurement of Skin Impedance

por

Simon Marcel Brunnuell

Esta dissertação foi julgada adequada para obtenção do título de

MESTRE EM ENGENHARIA ELÉTRICA

Área de concentração em "Sistemas Eletroeletrônicos"
e aprovada em sua forma final pelo

CURSO DE MESTRADO ACADÊMICO EM ENGENHARIA ELÉTRICA
DO CENTRO DE CIÊNCIAS TECNOLÓGICAS DA
UNIVERSIDADE DO ESTADO DE SANTA CATARINA.

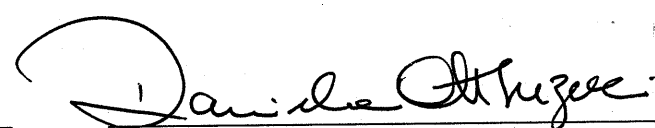
Banca Examinadora:



Prof. Dr. Pedro Bertemes Filho
CCT/UESC (Orientador/Presidente)



Prof. Dr. Aleksander Sade Paterno
CCT/UESC



Profa. Dra. Daniela Ota Hisayasu
Suzuki
UFSC

Joinville, SC, 15 de fevereiro de 2018.

SIMON MARCEL BRUNNQUELL

**DEVELOPMENT OF CARBON ELECTRODES FOR THE MEASUREMENT OF
SKIN IMPEDANCE**

Thesis presented to the Programa de Pos-Graduação em Engenharia Elétrica of the State University of Santa Catarina, Centro de Ciências Tecnológicas – CTT, as partial requirement for the achievement of the master degree in Engenharia Elétrica.

Supervisor: Prof. Dr. Pedro Bertemes-Filho
Co-Supervisor: Prof. Dr. Carla Dalmolin

**Joinville/SC
2018**

Brunnquell, Simon Marcel
Development of carbon fiber electrodes for the
measurement of skin impedance / Simon Marcel
Brunnquell. - Joinville , 2018.
91 p.

Orientador: Pedro Bertemes-Filho
Co-orientadora: Carla Dalmolin
Dissertação (Mestrado) - Universidade do Estado
de Santa Catarina, Centro de Ciências Tecnológicas,
Programa de Pós-Graduação em Engenharia Elétrica,
Joinville, 2018.

1. Bioimpedance. 2. Electrodes. 3. Carbon. 4.
Skin. I. Bertemes-Filho, Pedro. II. Dalmolin, Carla.
III. Universidade do Estado de Santa Catarina, Centro
de Ciências Tecnológicas, Programa de Pós-Graduação
em Engenharia Elétrica. IV. Título.

ACKNOWLEDGEMENTS

I would first like to thank my Supervisor Prof. Dr. Pedro Bertemes-Filho for giving me the opportunity to enroll in a master thesis opening in his laboratory and his practical guidance and support. For the practical help I would like to thank my co-supervisor Profa. Dr. Carla Dalmolin.

Special thanks go out to my girlfriend Sara Ferreira da Costa who was always encouraging me during the process of these studies. The same counts for my family and friends in Germany.

For the financial support I would like to thank the Coordenação de Aperfeiçoamento de Pessoal de Nível Superior (CAPES).

Last but not least, I would like to thank my dear colleagues and friends Sergio Fernandes Santos, Vinicius Grande Sirtoli, Kaue Felipe Morcelles, Douglas Dutra and all the staff members of the UDESC who helped me get along during my stay in Brazil.

ABSTRACT

Carbon electrodes show the advantage in comparison to metal electrodes that they are chemically inert and have a low impedance. Therefore, the aim of this work was to develop two impedance probes whose electrodes were based on carbon and to test their usability for the measurement of skin impedance. Knowing the passive electrical properties of skin is of importance e.g. for dosimetry purposes. The electrode material for one probe was graphite mixed into paraffin wax and for the other electrode carbon fibers that were glued together with silicone. The electrodes were formed concentric with an inner electrode and an outer ring electrode. Broadband frequency sweeps from 1 Hz to 1 MHz were conducted on the palm of the left hand of the author in a dry and a wet state. The impedance of dry skin at low frequencies lay above 100 k Ω , the high frequency value lay at a few hundred Ohms. One dominant dispersion could be observed. On wet skin a low frequency impedance in between 10 k Ω and 100 k Ω and a similar high frequency impedance as in the dry state was measured. From the measured impedance data the relative permittivity and the conductivity were calculated. The relative permittivity fell over the frequency range from around $7 \cdot 10^6$ to around 2,000 for dry skin and from around $35 \cdot 10^6$ to 2,000 for wet skin. Conductivity values ranged from 0.36 mS/m to 0.1 S/m and from 2.4 mS/m to 0.13 S/m, respectively. The possibility to fit the measured data to the Cole function, comparison with the literature data and simulations in "Finite Element Method Magnetics" (FEMM) showed the principle usability of the probes. Comparative measurements with an in house tetrapolar probe showed that the self made probes showed much less scattering of the measured values. This work contributes data of passive electric properties of palmar skin. Comparison with the literature data shows that these properties differ considerably from the skin electric properties in other parts of the body which should be considered in dosimetry simulations.

Keywords: Bioimpedance. Electrodes. Carbon. Skin.

RESUMO

Eletrodos de carbono mostram a vantagem em comparação com eletrodos metálicos na forma que eles são químicamente inertes e tem uma impedância baixa. Por isso, o objetivo deste trabalho foi desenvolver duas sondas de impedância cujos eletrodos se baseiam em carbono e testar suas usabilidades para a medição da impedância da pele. Conhecer as propriedades elétricas passivas da pele é importante, por exemplo, na área de dosimetria. O material utilizado para a fabricação de uma das sondas foi uma mistura de grafite e parafina e para a outra sonda fibras de carbono com silicone. Os eletrodos foram fabricados de maneira concêntrica de modo que há um eletrodo externo com um eletrodo interno. As varreduras de frequência de banda larga de 1 Hz a 1 MHz foram realizadas na palma da mão esquerda do autor, em estado seco e em estado úmido. A impedância da pele seca, em baixas frequências, situava-se acima de 100 k Ω e, o valor em altas frequências estava em poucas centenas de Ohms. Uma dispersão dominante pôde ser observada. Na pele úmida, foi medida uma impedância em baixas frequências entre 10 k Ω e 100 k Ω e uma impedância em altas frequências semelhante à do estado seco. A permissividade relativa caiu sobre a faixa de frequência de aproximadamente $7 \cdot 10^6$ para cerca de 2000 para a pele seca e de aproximadamente $35 \cdot 10^6$ para 2000 para a pele molhada. Os valores de condutividade variaram de 0,36 mS/m a 0,1 S/m e de 2,4 mS/m para 0,13 S/m, respectivamente. A possibilidade de ajustar os dados medidos à função Cole, a comparação com dados da literatura e simulações com a software “Finite Element Method Magnetics” (FEMM) mostrou a usabilidade principal das sondas. As medidas de comparação com uma sonda tetrapolar mostraram que as sondas autoproduzidas apresentam menos dispersão dos valores medidos. Este trabalho contribuiu com dados das propriedades elétricas passivas da pele palmar. A comparação com os dados da literatura mostra que essas propriedades diferem consideravelmente das propriedades elétricas da pele em outras partes do corpo e que isto deveria ser considerada em simulações por dosimetria.

Palavras-chave: Bioimpedância. Eletrodos. Carbono. Pele.

LIST OF FIGURES

| | |
|---|----|
| Figure 1 - Bode-plot over a frequency range of 10 Hz to 100 MHz: The values of the modulus $ Z $ are relative. | 27 |
| Figure 2 - Equivalent circuit representing the impedance of a biological tissue, where CPE denotes the constant phase element, ΔR the resistance of the tissue as described in 2.2 and R_∞ the resistance of the system at very high frequencies | 28 |
| Figure 3 - Example of a Cole plot: R_0 denotes the sum of R_∞ and ΔR . The angle α is a measure for the depression of the semiarc and $1/\tau$ denotes the characteristic frequency of the system i.e. the frequency where the reactance has its minimum in the Bode-plot..... | 28 |
| Figure 4 - Schematic of an electronic double layer on a metal electrode surface in an electrolyte solution | 31 |
| Figure 5 - Hemispherical electrode in contact with a volume conductor: The semicircles at r_v represent the equipotential lines | 33 |
| Figure 6 - Volume conductor in contact with electrodes A, B, C and D: The current I_{AB} is driven between electrodes A and B and current I_{CB} between C and D, respectively. The cross marks the point P at an arbitrary place within the volume conductor.... The square represents a volume within the volume conductor with a different resistivity than the rest of the conductor..... | 34 |
| Figure 7 - Microscopic photograph of the stratum corneum of a mouse ear..... | 37 |
| Figure 8 - Microscopic photograph of the stratum corneum of the foot palm of a guinea pig | 38 |
| Figure 9 - Overview of the skin structures | 39 |
| Figure 10 - Schematic representation of the three skin cancer types named in the text..... | 40 |
| Figure 11 - Side view of the electrode made from paraffin wax and graphite | 44 |
| Figure 12 – Cross section cut of the carbon fiber electrode: It shows the bundle of fibers in the central tube (1), the carbon fiber tissue of the outer electrode (2), the aluminum filling (3), the steel rods (4), the respective glass tubes for the electrodes (5) and the hot glue fixations (6). | 45 |
| Figure 13 - Top view of the electrode made of carbon fibers | 45 |
| Figure 14 - Side view of the electrode made of carbon fibers..... | 46 |

| | |
|---|----|
| Figure 15 - Impedance module at 37.7 kHz measured with the self made carbon fiber probe plotted against the resistivity of four different concentrations of saline solution | 47 |
| Figure 16 - Impedance module at 15.3 kHz measured with the tetrapolar probe plotted against the resistivity of four different concentrations of saline solution | 48 |
| Figure 17 - Model and measures for the numerical simulation of saline solution measured with the home made probe | 49 |
| Figure 18 - Calculated impedance values with FEMM plotted against the resistivities of four different concentrations of saline solution..... | 50 |
| Figure 19 - Schematic of the experimental setting | 51 |
| Figure 20 - Photograph of the tetrapolar probe used in this study | 52 |
| Figure 21 - Measurement site..... | 53 |
| Figure 22 – Module (above) and phase (below) of dry palmar skin measured with a probe made of paraffin and graphite (p/g), of carbon fibers and silicone (c/s) and a tetrapolar probe (4p) | 55 |
| Figure 23 - Module (above) and phase (below) of wet palmar skin measured with a probe made of paraffin and graphite (p/g), of carbon fibers and silicone (c/s) and a tetrapolar probe (4p) | 56 |
| Figure 24 – Relative permittivity (above) and conductivity (below) of dry palmar skin measured with a probe made of paraffin and graphite (p/g), of carbon fibers and silicone (c/s) and a tetrapolar probe (4p) | 58 |
| Figure 25 - Relative permittivity (above) and conductivity (below) of wet palmar skin measured with a probe made of paraffin and graphite (p/g), of carbon fibers and silicone (c/s) and a tetrapolar probe (4p) | 59 |
| Figure 26 - Dimensions of the skin model: The electrodes are shown in black | 61 |
| Figure 27 - Potential distribution and current density lines in the skin model at 100 Hz (a), 10 kHz (b) and 1 MHz (c): The color violet indicates 1 V and the color light blue 0 V. Each color indicates an interval of 50 mV..... | 63 |

LIST OF TABLES

| | |
|--|----|
| Table 1 - Measured values of the resistivity and the impedance of different saline solutions | 47 |
| Table 2 - Measured values of the resistivity and the impedance of different saline solutions | 48 |
| Table 3 - Measured resistivity and by simulation determined resistance values for different saline solutions..... | 49 |
| Table 4 - Fitting parameters for the Cole equation for each type of electrode..... | 60 |
| Table 5 - Fitting parameters for the Cole-Cole equation for each type of electrode..... | 61 |
| Table 6 - Material properties for the different layers of the skin model | 62 |
| Table 7 – Calculated real (R) and imaginary part (X) of the impedance of the skin model based on the values given in table 6 | 63 |
| Table 8 - Experimental values from this study and literature values of conductivity at three different frequencies | 68 |
| Table 9 - Experimental values from this study and literature values of relative permittivity at three different frequencies | 69 |
| Table 10 - Experimental values from this study and literature values of conductivity of wet skin at three different frequencies..... | 69 |
| Table 11 - Experimental values from this study and literature values of permittivity of wet skin at three different frequencies..... | 70 |
| Table 12 - Real (R) and the imaginary (X) part of the impedance as measured on dry skin with the carbon fiber probe and calculated with a numerical simulation in FEMM. All values are given in Ω | 70 |
| Table 13 - Comparison of the conductivity values (in mS/m) of the SC and the VS used for this simulation study and in the literature..... | 71 |
| Table 14 - Comparison of the relative permittivity values of the SC and the VS used for this simulation study and in the literature..... | 72 |

LIST OF ABBREVIATIONS

| | |
|-------|----------------------------|
| 4p: | Tetrapolar |
| AT: | Adipose tissue/subdermis |
| BBC: | Basal cell carcinoma |
| c/s: | Carbon fibers/silicone |
| MM: | Malignant Melanome |
| MUT: | Material under test |
| p/g: | Paraffin/graphite |
| RMSD: | Root-mean square deviation |
| SC: | Stratum Corneum |
| SCC: | Squameous cell carcinoma |
| VS: | Viable skin |

LIST OF SYMBOLS

| | |
|---------------------|--|
| B : | Susceptance |
| C : | Capacitance |
| f : | Frequency |
| G : | Conductance |
| I : | Current |
| j : | Imaginary number |
| k : | Geometric factor |
| R : | Resistance |
| ΔR : | Resistance of the parallel element in the Cole equation |
| R_{∞} : | Resistance at extremely high frequencies in the Cole equation |
| r_{el} : | Radius of electrode |
| V : | Voltage |
| X : | Reactance |
| Y : | Admittance |
| Z : | Impedance |
| $ Z $: | Impedance module |
| α : | Angle that indicates the depression of the arc in the Cole-Cole plot |
| ε^* : | Complex permittivity |
| ε_r^* : | Complex relative permittivity |
| ε_0 : | Electric field constant |
| φ : | Phase angle |
| ω : | Angular Frequency |
| π : | Pi |
| ρ : | Resistivity |
| σ : | Conductivity |
| τ : | Time constant |

TABLE OF CONTENTS

| | | |
|--------------|---|-----------|
| 1 | INTRODUCTION | 21 |
| 1.1 | GENERAL OBJECTIVE | 22 |
| 1.2 | SPECIFIC OBJECTIVES..... | 22 |
| 2 | BIOIMPEDANCE SPECTROSCOPY BASICS | 23 |
| 2.1 | BASIC CONCEPTS | 23 |
| 2.2 | BIOLOGICAL PHENOMENA IMPEDING CURRENT..... | 25 |
| 3 | ELECTRODE IMPEDANCE..... | 31 |
| 3.1 | MECHANISMS AT THE ELECTRODE SURFACE | 31 |
| 3.1.1 | Double layer | 31 |
| 3.1.2 | Faradaic processes | 32 |
| 3.2 | REDUCING ELECTRODE EFFECTS ON THE IMPEDANCE SPECTRUM..... | 32 |
| 3.3 | FIELD DISTRIBUTION AND SENSITIVITY | 33 |
| 4 | SKIN IMPEDANCE..... | 37 |
| 4.1 | SKIN STRUCTURE..... | 37 |
| 4.2 | IMPEDANCE OF HEALTHY AND CANCEROUS SKIN..... | 39 |
| 4.3 | ACCESSING SKIN IMPEDANCE | 41 |
| 5 | EXPERIMENTS AND RESULTS | 43 |
| 5.1 | MICROELECTRODE FABRICATION | 43 |
| 5.1.1 | Paraffin wax with graphite | 43 |
| 5.1.2 | Carbon fibers with silicone | 44 |
| 5.2 | CALIBRATION PROCEDURE OF THE ELECTRODE | 46 |
| 5.2.1 | Experimental measurements | 46 |
| 5.2.2 | Numerical simulation | 48 |
| 5.3 | SKIN IMPEDANCE MEASUREMENT | 50 |
| 5.4 | RESULTS | 53 |

| | |
|--|-----------|
| 5.4.1 Impedance | 53 |
| 5.4.1.1 Dry skin..... | 53 |
| 5.4.1.2 Wet skin..... | 55 |
| 5.4.2 Permittivity | 57 |
| 5.4.2.1 Dry skin..... | 57 |
| 5.4.2.2 Wet skin..... | 58 |
| 5.4.3 Parameters of the fitting | 59 |
| 5.5 NUMERICAL SIMULATION OF THE SKIN IMPEDANCE WITH FEMM | 61 |
| 6 DISCUSSIONS | 65 |
| 6.1 DETERMINATION OF THE PROBE FACTOR | 65 |
| 6.2 SKIN IMPEDANCE MEASUREMENT..... | 65 |
| 6.3 SIMULATION OF SKIN IMPEDANCE | 70 |
| 7 CONCLUSION AND PROPOSALS FOR FUTURE WORKS | 75 |
| 7.1 CONCLUSION | 75 |
| 7.2 PROPOSALS FOR FUTURE WORKS | 75 |
| REFERENCES | 77 |
| APPENDIX A: Technical specifications of the probes of this study compared to literature | 87 |
| APPENDIX B: Protocol of the FEMM modeling for the skin impedance at 1 MHz | 88 |

1 INTRODUCTION

Impedance spectroscopy is a simple tool to investigate the electrical properties of materials and thereby draw conclusions of the state of them. In this technique an alternating current or voltage of low intensity is applied to the material, the respective voltage or current measured and finally the frequency dependent resistance, the impedance, calculated.

The technique of impedance spectroscopy is also applied on biological material and used for example for the assessment of meat quality (PLIQUETT, 2010), for cell culture monitoring (EDMONDSON et al., 2014; LEI; WU; HUANG, 2015) or for diagnostic purposes of differentiating between healthy and pathogenic tissues.

A special application is the cancer diagnosis, especially for skin cancer (MALVEHY et al., 2014; MOHR et al., 2013). The noninvasive nature of this technique gives a competitive edge over other diagnostic methods. The main difference in between healthy and cancerous tissue is the much higher resistivity of cancerous tissue at low frequencies (HAEMMERICH et al., 2003, 2009; PRAKASH et al., 2015). Clinical studies have already been conducted with a special probe type where the surface of the electrodes is covered with microscale needles that penetrate the stratum corneum (MALVEHY et al., 2014; MOHR et al., 2013). These types of electrodes lower the recorded skin impedance and in case of electrocardiogram measurements they reduce the movement artifacts (DIAS et al., 2010; ZHANG et al., 2016).

However, it could be shown that with noninvasive electrodes the differences between benign nevi and basal cell carcinoma (BCC) are more accentuated than with the micro invasive electrodes (ABERG et al., 2005). Furthermore, there is the risk of remnant needles in the skin.

A new material that can be considered for noninvasive electrodes is conductive rubber. There are already commercially available electrodes for the recording of electrocardiograms, but for broadband bioimpedance spectroscopy there is limited available literature (KAUFMANN; ARDELT; RYSCHKA, 2013). These carbon rubber electrodes have the advantage over other dry for their simple fabrication and their versatility to adapt to the topology of the skin surface topology. Moreover there is a lower need for electrolytic gels that can cause an extra potential in between the electrode surface and the gel itself (PENG et al., 2015a; YAO; ZHU, 2016).

Another point concerning skin impedance is its importance when it comes to electromagnetic compatibility since the skin is the organ with which humans are in direct

contact with their environment. Especially for frequencies below 100 Hz there is little literature data available. So validation of the data at hand (YAMAMOTO; YAMAMOTO, 1976) might be important to investigate electromagnetic field exposure (DE SANTIS et al., 2015, 2016; SCHMID; CECIL; ÜBERBACHER, 2013; SCHMID; HIRTL, 2016)

1.1 GENERAL OBJECTIVE

The aim of this study is to develop an impedance probe made of carbon material for the measuring skin impedance.

1.2 SPECIFIC OBJECTIVES

Firstly, the homemade probe will be calibrated with a saline solution with different concentrations of NaCl. These results will be compared to numerical simulations in FEMM. The resultant geometric factor of the probe will also be compared with the analytically calculated value.

Secondly, an in-vivo experiment on the left hand palm tissue will be conducted by using a broadband impedance meter over a frequency range from 1 Hz to 1 MHz. The relative complex permittivity and conductivity of the hand will be calculated.

Third, the results will be checked for a potential match with both Cole and the Cole-Cole models and then compared to literature data.

Finally, the skin impedance will be modeled using FEMM and then compared to experimental data and published data from literature.

2 BIOIMPEDANCE SPECTROSCOPY BASICS

2.1 BASIC CONCEPTS

In bioimpedance spectroscopy an alternating current (I) of constant amplitude in different frequencies is applied to the material under test (MUT). A voltage (V) is recorded and then an impedance (Z) is calculated according to Ohm's law, as

$$Z(\omega) = \frac{V(\omega)}{I(\omega)} \quad (1)$$

where ω denotes the angular frequency, which is equal to $2\pi f$.

The current can either be applied as a sinusoidal waveform at discrete frequencies, as a square pulse, a chirp or as a multisignal in the form of a noise.

The impedance Z is a complex number, that can be characterized by its modulus $|Z|$ and its phase angle φ , that indicates the phase shift between V and I :

$$Z(\omega) = |Z|e^{j\varphi} \quad (2)$$

The impedance Z as a complex number takes dissipative, i.e. resistive, and capacitive as well as inductive elements into account. Inductive elements are not common in biological material. Resistive means that charge carriers are moved along the electric field. Thereby heat is dissipated which impedes the movement of the charge carriers. Capacitive means that there is no net flow of charges but these charges are displaced within the dielectric and thereby energy can be stored. Due to the storage of charge at the capacitor plates the current in respect to the voltage is delayed, causing the phase shift. Equation (2) can be written like

$$|Z| = \sqrt{R^2 + X^2} \quad (3)$$

$$\varphi = \arctan(X/R) \quad (4)$$

where R is called resistance or the real part of the impedance which is associated with dissipative losses.

It can be calculated by taking the voltage, where the current passing through the MUT is maximal (V_{Imax}) and dividing by the maximal current (I_m) or by Euler's formula:

$$R = \frac{V_{Imax}}{I_m} = |Z|\cos(j\varphi) \quad (5)$$

X is the reactance and comprises the imaginary part of systems, which are composed only of capacitance. It can be calculated by dividing the voltage at the point where the current is zero, V_{Imin} , by I_m or by Euler's formula:

$$X = \frac{V_{Imin}}{I_m} = |Z|\sin(j\varphi) \quad (6)$$

Both $|Z|$ and φ , as a function of frequency, can be plotted in a Bode plot.

X can further be characterized by the capacitance of the MUT by the following equation:

$$X = \frac{1}{\omega C} = \frac{k}{\omega \varepsilon_r \varepsilon_0} \quad (7)$$

where ε_r is the relative permittivity of the Medium through which the current passes, ε_0 is the permittivity of free space, also called the dielectric constant ($8,85 \cdot 10^{-12}$ F/m) and k the geometric factor of the MUT. The permittivity ε is a measure for the permeability of the medium for electric fields.

According to the formula of Euler, Z can then also be represented as

$$Z = R + jX = \rho k = k(\rho' + j\rho'') \quad (8)$$

where ρ is the resistivity of the MUT, which can be separated in a real and an imaginary part.

The admittance Y is the reciprocal of Z and can be subdivided into a real part, the conductance G , and an imaginary part, the susceptance B .

$$Y = \frac{1}{Z} = G + jB = \frac{1}{k\rho} = \frac{\sigma}{k} \quad (9)$$

$$G = \frac{R}{R^2 + X^2} = \frac{\sigma'}{k} = \frac{\rho'}{k|\rho|^2} \quad (10)$$

$$B = \frac{X}{R^2 + X^2} = \frac{\sigma''}{k} = \frac{\rho''}{k|\rho|^2} \quad (11)$$

Since the impedance is also dependent on the geometry of the electrodes, for comparison of different materials it is better to present their electrical properties in terms of permittivity. The complex permittivity can be derived from the following equation when σ is known:

$$\varepsilon^* = \varepsilon_r^* \varepsilon_0 = \frac{\sigma}{j\omega} = \varepsilon' - j\varepsilon'' \quad (12)$$

$$\varepsilon' = \frac{\sigma''}{\omega} = \frac{\rho''}{\omega|\rho|^2} \quad (13)$$

$$\varepsilon'' = \frac{\sigma'}{\omega} = \frac{\rho'}{\omega|\rho|^2} \quad (14)$$

where ε' describes the ability of the material to store energy and ε'' the dielectric losses, which means energy losses due to heat dissipation during the polarization process.

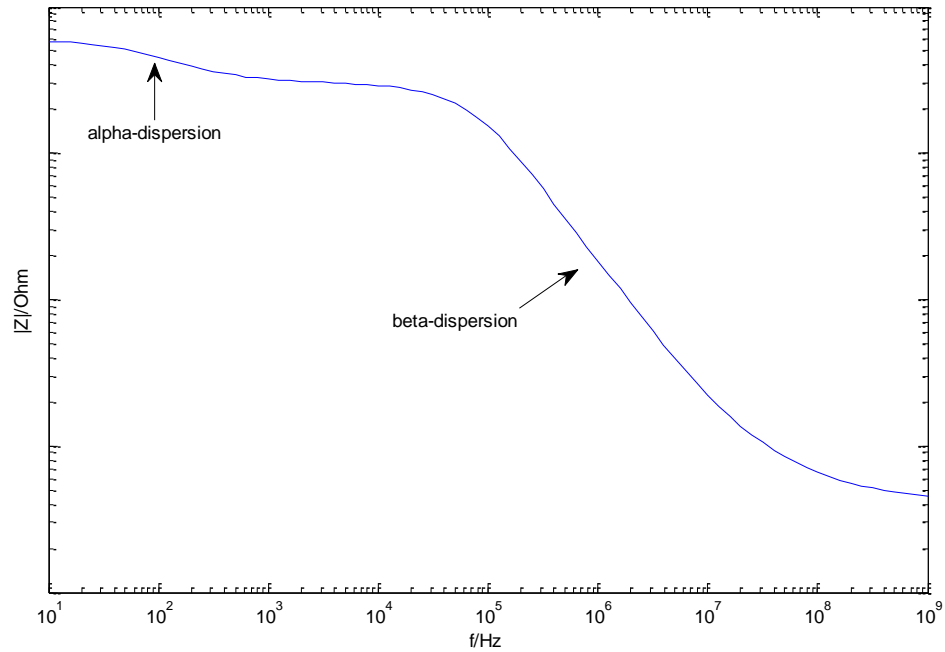
2.2 BIOLOGICAL PHENOMENA IMPEDING CURRENT

The dissipative elements in bioimpedance spectroscopy can be referred to the electrolytic conductivity of the extracellular and intracellular medium. It was found out, that the intracellular conductivity of cell bodies in aplysia neurons comprises only 5% of the conductivity of physiological saline or seawater (CARPENTER; HOVEY; BAK, 1973). Similar values were found in other cell types (CARPENTER; HOVEY; BAK, 1975). Investigations with ion selective electrodes showed that the activity of potassium ions in soma of aplysia neurons is similar to that in seawater (KUNZE; BROWN, 1971). Measurements in barnacle muscle fibers (HINKE, 1980; HINKE; CAILLÉ; GAYTON, 1973), in mouse EDL muscle (DONALDSON; LEADER, 1984) as well as in giant squid axons (FONG; CHANG, 1988) showed also relatively high activity of potassium. This indicates that potassium, which is the most abundant ion in the intracellular space, is free to move, whereas sodium was considered to be bound (HINKE; CAILLÉ; GAYTON, 1973). Measurements of ionic activity in concentrated protein solutions showed stronger binding of sodium than that of potassium, as well (REBOIRAS; PFISTER; PAULY, 1978). Therefore, water structure and high viscosity could impede the intracellular conductivity, as it was supposed by Carpenter et al. (1973, 1975) and as it was estimated by Pauly (PAULY, 1973). Measurements of the potassium activities with ion selective electrodes in epithelial cells, however, showed much lower values (LING, 1984), indicating binding or compartmentalization also of potassium ions within the cell. Other noninvasive techniques showed considerable lower activities than in saline solution in muscle cells (ACKER; PIETRUSCHKA; ZIEROLD, 1985; LEE, 1975; MAUGHAN; RECCHIA, 1985) and in bacteria (COPE; DAMADIAN, 1970). To sum up, whereas in red blood cells, that represent a very simple form of cells, the high viscosity of cellular water could be the main reason for the high resistivity (PAULY, 1973), in more complex cell types ion binding contributes to the resistivity, too. The high activity values for potassium ions in muscle cells, as mentioned above, can probably be attributed to destruction of the internal structure of these cells (EDELMAAN, 1989). Since the extracellular matrix (ECM) consists of proteins (mainly collagen fibers) and glycosaminoglycans (e.g. hyaluronic acid) (MOUW; OU; WEAVER, 2014) that offer charged surfaces, too, binding of ions in the ECM and thereby restricting the ionic mobility can be assumed for the extracellular, as well.

Apart from that, instead of only regarding ionic conductance in tissues, it was shown that fibrous tissues behave electrically as semiconductors. One mechanism that plays a role in the conduction mechanism is the hopping of protons from one water molecule to the next according to the Grotthus-mechanism (AGMON et al., 2016; GASCOYNE; PETHIG; SZENT-GYÖRGYI, 1981; ORDINARIO et al., 2014; PETHIG, 1988; SASAKI, 1984). Electronic conduction was also proposed for collagen (BARDELMEYER, 1973; GAUZA; KUBISZ, 2011; TOMASELLI; SHAMOS, 1974).

The capacitive elements cause a phase shift in between excitation and system response. Phase shifts in biological materials are caused e.g. by polarization phenomena at phospholipid membranes or fixed charged surfaces at polyelectrolytes like proteins for example (BORDI; CAMETTI; COLBY, 2004). Another cause is the dielectric relaxation of globular proteins and colloidal particles (PETHIG; KELL, 1987; SCHWAN et al., 1962; WOLF et al., 2012). Due to these mechanisms over a frequency range from 10 Hz to 10 MHz biological materials exhibit two dispersions in their impedance spectra. The so called alpha-dispersion occurs between 10 Hz and 1 kHz and is generally referred to polarization phenomena at surface charges of the cell, but in the case of tissue impedance the surface charges of fibrous proteins in the extracellular matrix probably contribute to this dispersion as well, which can be shown for model systems like polyelectrolyte solutions (BORDI; CAMETTI; COLBY, 2004). That the extracellular matrix is mainly contributing to the alpha-dispersion can be concluded from experiments with blood, that does not show this kind of dispersion (BOTHWELL; SCHWAN, 1956; GABRIEL; LAU; GABRIEL, 1996; WOLF et al., 2011). On the other hand, the beta-dispersion, that occurs at frequencies between 100 kHz and 10 MHz, is commonly referred to polarization phenomena at the lipid double layer of the cell membrane but it has also been shown that orientation polarization of globular proteins occur in this frequency range (PETHIG; KELL, 1987; WOLF et al., 2012). Another interpretation of the beta-dispersion can be drawn from experiments where water contents of tendon tissue were varied. With increasing water content the permittivity of the system was increasing to very high values (over 10^6). This indicates a role of water in the dispersion phenomenon since contribution of cells could be excluded and rotational motion of the proteins seems improbable (GULINO et al., 2005). Figure 1 shows an example of a Bode plot of a tissue to visualize the alpha- and beta-dispersion.

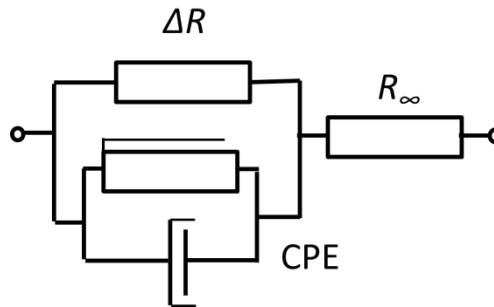
Figure 1 - Bode-plot over a frequency range of 10 Hz to 100 MHz: The values of the modulus $|Z|$ are relative.



Source: <http://niremf.ifac.cnr.it/tissprop/htmlclie/htmlclie.php> Access:12/8/2016

The properties of biological materials within a frequency range, in which one single dispersion occurs, can be modeled as two resistors ΔR and R_∞ in series, which represent the resistances of the intra- and extracellular medium, respectively (see Figure 2). One constant phase element (CPE) is in parallel with the resistor that represents the intracellular resistance. A CPE can be modeled as a frequency dependent resistance R_{CPE} in series with a frequency dependent reactance X_{CPE} .

Figure 2 - Equivalent circuit representing the impedance of a biological tissue, where CPE denotes the constant phase element, ΔR the resistance of the tissue as described in 2.2 and R_∞ the resistance of the system at very high frequencies

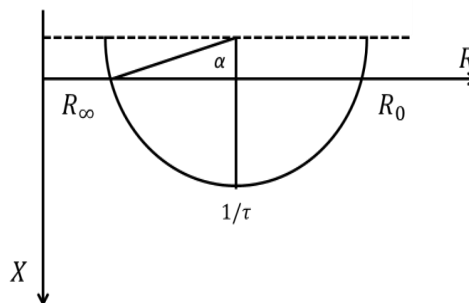


Source: Author

This circuit can mathematically be described by the Cole equation where the exponent α describes the depression of the arc (COLE, 1940) and τ is a normalization factor in the form of a time constant. Figure 3 shows the resulting Nyquist plot.

$$Z(\omega) = R_\infty + \frac{\Delta R}{1 + (j\omega\tau)^\alpha} \quad (15)$$

Figure 3 - Example of a Cole plot: R_0 denotes the sum of R_∞ and ΔR . The angle α is a measure for the depression of the semiarc and $1/\tau$ denotes the characteristic frequency of the system i.e. the frequency where the reactance has its minimum in the Bode-plot



Source: Author

This exponent α probably has its physical origin in the distribution of relaxation times as it occurs in inhomogeneous media like biological materials (SALTER, 1978). It can also be interpreted as storage of energy of hopping charges absorbed or bounded within a network like in a semiconductor (JONSCHER, 1977). When the values of the complex permittivity instead of the impedance are presented, these values can be described by the Cole-Cole equation (COLE; COLE, 1941).

$$\varepsilon^*(\omega) = \varepsilon_\infty + \frac{\varepsilon_0 - \varepsilon_\infty}{1 + (j\omega\tau)^{1-\alpha}} \quad (16)$$

The next chapter deals with electrodes and the following one with the applicability of the concepts presented in this chapter on skin impedance

3 ELECTRODE IMPEDANCE

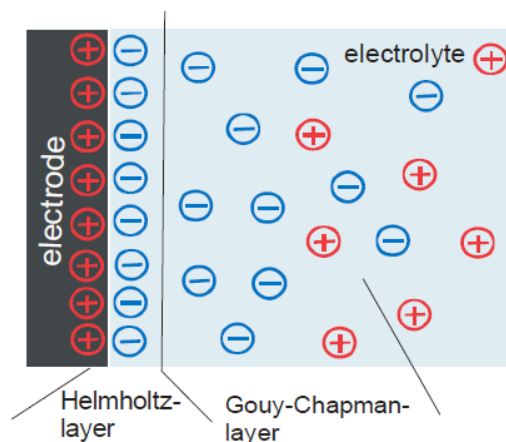
3.1 MECHANISMS AT THE ELECTRODE SURFACE

When it comes to assessing the electrical properties of biological material, the interface is of critical importance. Electrodes form this interface as a connection of ionic and electronic conductors. In principle, it is a piece of electronic conductor dipped into an electrolyte. When an electrode comes into contact with an ionic solution there are two processes which occur at the interface.

3.1.1 Double layer

One process is the buildup of a double layer when atoms of the electrode become ionized and solvated counterions from the solution adsorb at the surface. This layer is called Helmholtz layer. Farther away from the electrode surface there is a diffusive layer of these counterions which is called Gouy-Chapman layer. This is not of importance at physiological ion concentrations (Fig 4). The specific capacitance of the electrode surface can be calculated by dividing the surface charge density by the product of the field strength and the thickness of the Helmholtz-layer.

Figure 4 - Schematic of an electronic double layer on a metal electrode surface in an electrolyte solution



Source: PLIQUETT et al. (2010)

3.1.2 Faradaic processes

A faradaic current exists when a charge transport occurs at the electrode surface. The resistance this current senses is called charge transfer resistance. In those processes an ionic species is adsorbed on the electrode surface. The adsorption on the electrode surface implies that a charge is stored which gives rise to the pseudocapacitance. The pseudocapacitance can be explained for example with the adsorption of a proton on a platinum surface (CONWAY; BIRSS; WOJTOWICZ, 1997). This process is called underpotential deposition since the adsorption of a species different from the electrode material can already take place at electrode potentials lower than those necessary for the adsorption of the proper ions. The pseudocapacitance of polyaniline for example comprises values between 135 and 168 $\mu\text{F}/\text{cm}^2$ depending on the electrolyte (EFTEKHARI; LI; YANG, 2017). In comparison the value of the double layer capacitance lies between 15 and 50 $\mu\text{F}/\text{cm}^2$.

3.2 REDUCING ELECTRODE EFFECTS ON THE IMPEDANCE SPECTRUM

According to eq. (7) the capacitive impedance increases with decreasing capacitance. Thereby the influence of the electrode impedance becomes more influential on the impedance spectrum the smaller the electrode surface gets and therefore higher frequencies are necessary to circumvent this effect. This can become a range limiting effect for bioimpedance measurements. To circumvent influences of electrode polarization, a second pair of electrodes can be placed in between or away from the current driving electrodes. When a voltage measurement system with a high input impedance is used, almost no current flows over the electrode surface and thereby no electrode effects occur (GEDDES, 1996). The measured impedance is then called transfer impedance.

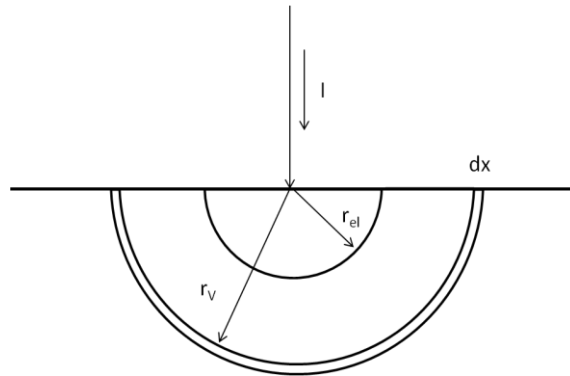
Another possibility is to enlarge the electrode surface and thereby to reduce the capacitive impedance. This can, for example, be done by platinizing the surface or using of materials made out of carbon, such as conductive polymers and graphite. Conductive polymers are especially interesting for the use of bioimpedance measurements because contrary to platinum black they are biocompatible (MALLEO et al., 2010). It has already been shown by Chen et al. (2013) that the coating with PEDOT minimizes the capacitive impedance of minimally invasive gold electrodes. By doping the PEDOT with SDS the

impedance could further be lowered (WU et al., 2015). Similar effects could be yielded by coating of gold electrodes with carbon nanotubes in a bioimpedance platform for cell culturing (SRINIVASARAGHAVAN et al., 2014).

3.3 FIELD DISTRIBUTION AND SENSITIVITY

When an electrode is in contact to a volume conductor the current I is transmitted from the electrode and distributes into the medium. The potential in the conductor distributes according to the current density, which has the highest value directly at the electrode and then decreases with increasing distance. In the case of a hemispherical electrode (PLIQUETT et al., 2010), the differential voltage drop dV around the electrode within thickness dx at a distance x away from the electrode will be:

Figure 5 - Hemispherical electrode in contact with a volume conductor: The semicircles at r_v represent the equipotential lines



Source: Author

$$dV = \frac{\rho I}{2\pi x^2} dx \quad (17)$$

Integrating over the distance from the electrode surface $r_v - r_{el}$ gives

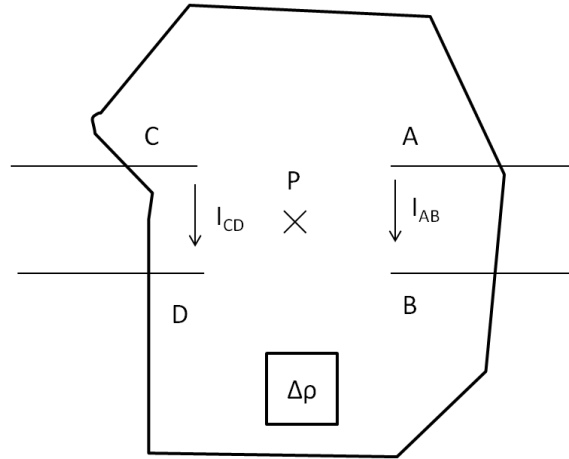
$$V = \frac{\rho I}{2\pi} \int_{r_{el}}^{r_v} \frac{1}{x^2} dx = \frac{\rho I}{2\pi} \left(\frac{1}{r_v} - \frac{1}{r_{el}} \right) \quad (18)$$

where r_v is the radius of a hemisphere in the volume and r_{el} is the radius of the electrode.

It shall be mentioned here that in the case of a monopolar disc shaped electrode, the potential drop from the electrode follows the following equation (NEWMAN, 1966)

$$V = \frac{\rho I}{4r_{el}} \quad (19)$$

Figure 6 - Volume conductor in contact with electrodes A, B, C and D: The current I_{AB} is driven between electrodes A and B and current I_{CD} between C and D, respectively. The cross marks the point P at an arbitrary place within the volume conductor. The square represents a volume within the volume conductor with a different resistivity than the rest of the conductor.



Source: Author

In the bipolar case, when a current is driven between an electrode A and B the voltage drop V_{AP} at a point P within the volume with respect to A is

$$V_{AP} = \frac{\rho I}{2\pi r_{AP}} \quad (20)$$

The situation is similar at a point P with respect to B, only that here the current is negative at the electrode (BERTEMES-FILHO, 2002).

$$V_{BP} = \frac{-\rho I}{2\pi r_{BP}} \quad (21)$$

This means that at points where the equipotential line reaches zero, no resistance can be measured there by an additional recording electrode.

The potential at point P can then be calculated by adding the two contributions.

$$\Phi_P = \frac{I\rho}{2\pi} \left(\frac{1}{r_{AP}} - \frac{1}{r_{BP}} \right) \quad (22)$$

The potential at point P can also be written as a scalar product if AB is considered very small in relation to the distance to P.

$$\Phi_P = \frac{I\rho}{2\pi|r|^2} \overrightarrow{L_{AB}} \cdot \overrightarrow{r_e} \quad (23)$$

where \vec{L}_{AB} is the vector that connects the points A and B, \vec{r}_e is the unity vector of r_e that directs to P and $|r|$ is the absolute value of r_e .

Assuming an electrode pair CD that is picking up the voltage generated by the current I in between A and B, instead of a unipolar electrode, then equation 23 becomes

$$V_{CD} = \frac{I\rho}{2\pi} \left(\frac{\vec{L}_{AB} \cdot \vec{L}_{CD}}{|r|^3} \right) \quad (24)$$

By dividing through I one obtains the transfer impedance Z.

$$Z = \frac{\rho}{2\pi|r|^3} \vec{L}_{AB} \cdot \vec{L}_{CD} = \vec{H} \cdot \vec{L}_{CD} \quad (25)$$

where \vec{H} is called the lead vector.

In the case of the four electrodes in line, the potential at point D has to be subtracted from the one at point C (see equation 22).

$$V_{CD} = \frac{I\rho}{2\pi} \left(\frac{1}{r_{AC}} - \frac{1}{r_{AD}} + \frac{1}{r_{BD}} - \frac{1}{r_{BC}} \right) \quad (26)$$

In some cases, where the electrodes are not coplanar, and H cannot be determined analytically, the concept of reciprocity theorem can be used (GESELOWITZ, 1971). When a homogeneous medium that is connected to two pairs of electrodes the ratio of potential applied and current flowing in between one electrode pair is the same as for the other electrode pair. Then, according to equations 19 and 25, Z yields:

$$Z = \rho \iiint \frac{\vec{J}_{AB} \cdot \vec{J}_{CD}}{I_{AB}I_{CD}} dV = \rho \iiint S dV \quad (27)$$

where S is called sensitivity and

$$\vec{J} = \frac{I}{2\pi|r|^2} \vec{r}_e \quad (28)$$

When a change in resistivity in a region within the volume conductor changes ($\Delta\rho$) then the change in transfer impedance ΔZ yields

$$\Delta Z = \Delta\rho \iiint \frac{(\vec{J} + \Delta\vec{J})_{AB} \cdot \vec{J}_{CD}}{I_{AB}I_{CD}} dV \quad (29)$$

This means the sensitivity of a measurement is the ability to detect a change in impedance due to a change of the resistivity of an area within a volume conductor. When the

two vectors \vec{J}_{AB} and \vec{J}_{CD} span an angle more than 90° , the sensitivity in this field will be negative (BROWN; WILSON; BERTEMES-FILHO, 2000).

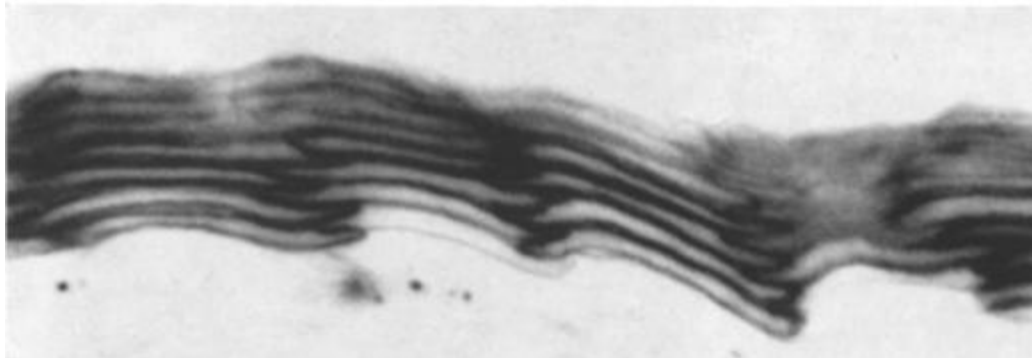
There has been some effort to avoid negative sensitivity fields for example by putting a hydrogel in between MUT and electrode (BERTEMES-FILHO et al., 2003) or doing a second measurement perpendicular to the first and adding the two measurements so that the negative sensitivity can be compensated (ABIR; RABBANI, 2014; ABIR et al., 2013; RABBANI et al., 1999; RABBANI; KARAL, 2008). This method is called the focused impedance measurement (FIM), where the sensitivity field can be restricted to the area between the electrodes. This method has not yet been used for the detection of skin cancer. Apart from negative sensitivity areas there are other error sources when measuring with tetrapolar probes (GRIMNES; MARTINSEN, 2006). Therefore, it is preferable to use bipolar or monopolar measurements for high impedance materials like skin tissue. The next chapter deals with anatomical reasons for the skin impedance and how it presents itself.

4 SKIN IMPEDANCE

4.1 SKIN STRUCTURE

Skin is composed of the epidermis, dermis and subcutis or hypodermis layer. The outermost part of the epidermis is the stratum corneum (SC), consisting of highly keratinized dead cells, also known as the keratinocytes. The intercellular space is filled with different types of lipids (BOUWSTRA et al., 2003). This layer serves as a mechanical and chemical barrier and has a thickness of round about 14 μm (BIRGERSSON et al., 2011) with about ten cell layers (YA-XIAN; SUETAKE; TAGAMI, 1999), but can comprise several millimeters at the sole of the foot. The keratinocytes are in general ordered in a columnar structure, as it can be seen in Figure 7.

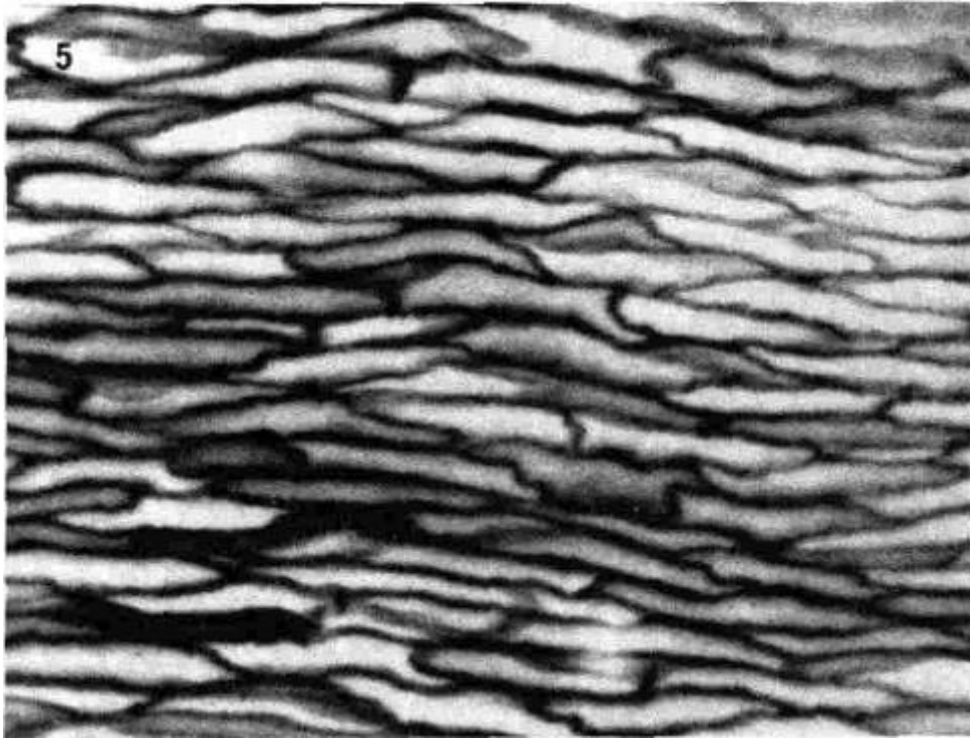
Figure 7 - Microscopic photograph of the stratum corneum of a mouse ear



Source: (CHRISTOPHERS, 1971a)

On the palm of the hands and on the foot soles, the SC is less ordered and lacks the columnar structure (Fig 9). Furthermore, only in these areas there is a stratum lucidum as depicted in Fig 10.

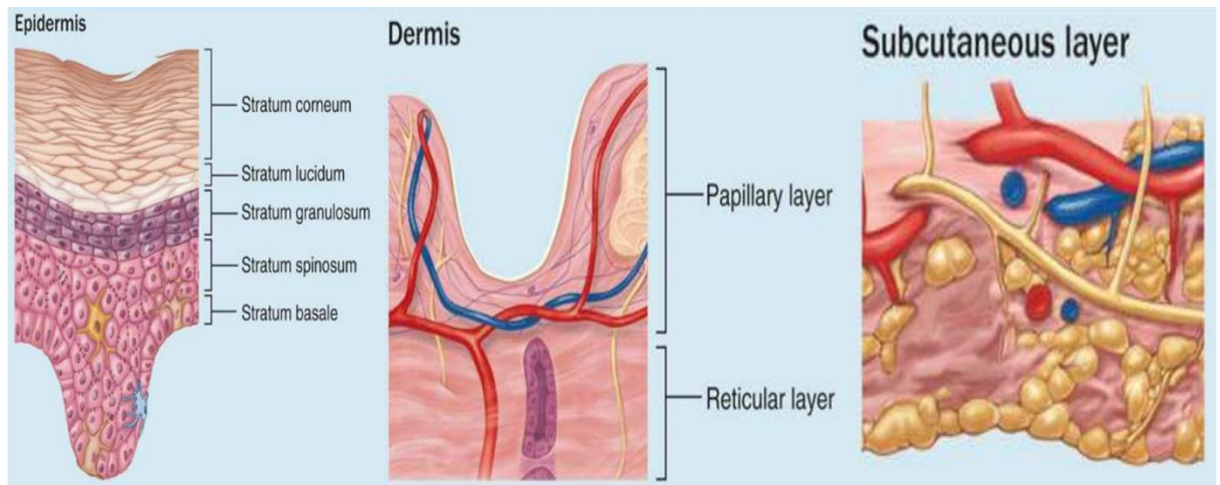
Figure 8 - Microscopic photograph of the stratum corneum of the foot palm of a guinea pig



Source: (CHRISTOPHERS, 1971b)

Below the SC, the keratinization decreases with increasing depth. The lowest layer of the Epidermis is the stratum basale. The stratum basale itself is the place of the melanocytes, which contain melanin (the skin pigment). This layer consists of dividing cells that wander to the surface. The dermis is a vascularized layer consisting of connective tissue with collagen fibers synthesized by fibroblasts. This layer is the place of the hair follicles and the sweat ducts. The lowest layer is the subdermis which mainly consists of adipose tissue and has the task of buffering mechanical pressure on the skin.

Figure 9 - Overview of the skin structures



Source: MESCHER, 2013

4.2 IMPEDANCE OF HEALTHY AND CANCEROUS SKIN

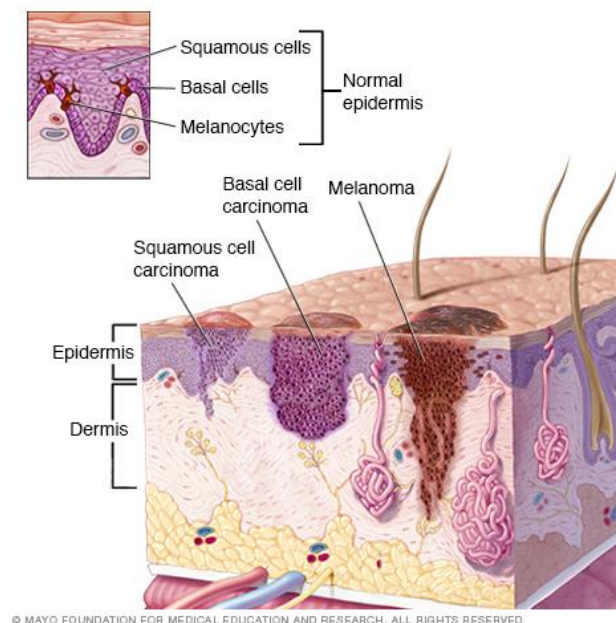
The impedance of the skin fits relatively well to the Cole equation (15) so it can be described by the parameters ΔR , R_∞ , τ and α . It was shown in a skin stripping experiment by Yamamoto and Yamamoto (1976) that the dielectric dispersion of the skin decreases as the SC is more stripped off. The experiments suggest that the value of ΔR represents the resistance of the SC and R_∞ represents the resistance of the viable skin that comprises the epidermis apart from the SC and dermis. Stripping experiments executed (BIRGERSSON et al., 2013) showed that the SC acts as a nonconductive dielectric with a resistivity between approximately 300 and 0.4 k Ω m from 1 kHz to 1 MHz and a relative permittivity that decreases from a value of 250 to 50 in the same frequency range. On the contrary, the viable skin showed a relatively stable low resistivity between 3 and 1 Ω m and a decreasing relative permittivity from 1.5 million to 200 over the same frequency range. The exponent α is supposed to be related to the hydration state of the SC (SALTER, 1981).

It should be mentioned that, in real skin, there are some aberrations from the Cole (Equation 15) or the Cole-Cole behavior (Equation 16). At high frequencies the circular arc bends over, but this aberration decreases when the SC is stripped off (YAMAMOTO; YAMAMOTO, 1976). In order to get a better fit of this behavior at high frequencies, the model of the so called “universal dielectric response” (JONSCHER, 1975, 1977) may be applied, that includes a second exponent. Moreover, in the case of skin, sweat ducts alter the conductivity of the skin over time. That’s why a slightly different model was introduced by Grimnes and Martinsen (GRIMNES; MARTINSEN, 2005) which they called as “Free

Conductance Model”. Here the constant phase element is in parallel to a variable resistance (or conductance) R_{var} . Recently, it was found that the sweat ducts can better be modelled by a memristor (JOHNSEN, 2012; JOHNSEN et al., 2011). However, for the scope of this work, it will be sufficient to stick to the Cole model.

Cancerous tissue differs from healthy tissue in terms of uncontrolled growth and cell division. For example, the most common skin cancers, the BCC, cells, that are located in the stratum basale, begin to divide without any restriction and further keratinization that is typically found in healthy skin tissue. The second most common form is the squamous cell carcinoma (SCC) which develops in layers above the stratum basale (LACY; ALWAN, 2013; NOURI, 2008; PASTUSHENKO et al., 2014). The malignant melanoma (MM) is a degeneration of melanocytes located in the stratum basale, which is much less common than the previously named ones but more devastating and non-curable cancer type in its advanced stage (FOLETTTO; HAAS, 2014) (Figure 10). Further differences lie in its enormous vascularization (PASTUSHENKO et al., 2014) and metabolic abnormalities. The phenotypical differences can also be connected to altered electric properties.

Figure 10 - Schematic representation of the three skin cancer types named in the text



Source: http://www.mayoclinic.org/-/media/kcms/gbs/patient-consumer/images/2013/11/15/17/40/ds00190_-ds00439_-ds00924_-ds00925_im02400_c7_skincancerthu_jpg.ashx Access: 03/11/2017

For example it is known that Ehrlich ascite tumor cells contain less protein than normal cells and have an intracellular conductivity close to saline solution (PAULY, 1963).

Less ion binding due to less protein content could therefore be responsible for the higher intracellular conductivity of cancer cells. There is a great amount of literature that proves that most of the cellular water is bound to proteins or in some way structured (CLEGG, 1984; LING; WALTON, 1976; POLLACK; CAMERON; WHEATLEY, 2006). Water structuring in collagen which accounts for most parts of the dermis could be proven by dielectric spectroscopy (GULINO et al., 2005; KURZWEIL-SEGEV et al., 2017). On the other hand, water in cancer tissue is less structured than in normal tissue which is the principle of tumor diagnosis by MRI (AKBER, 2008; DAMADIAN, 1971). Decreased collagen bundle orientation in breast cancer and BBC tissue could be observe with second harmonic generation microscopy (AJETI et al., 2011; BROWN et al., 2003; LIN et al., 2006) that could support water orienting. As a resume, it can be assumed that less structuring of water of cancer tissue might add to the higher conductivity of it by decreasing the viscosity. Additionally, cancer cells pull their energy mainly out of the glycolysis mechanism that produces pyruvate that further adds to a higher conductivity (ZHENG, 2012). Also the high acidity of the extracellular environment (KATO et al., 2013; ROFSTAD et al., 2006) and the abnormally high vascularization (PASTUSHENKO et al., 2014) contribute to a higher conductivity of cancerous tissue. Another factor could be that the ECM of tumor tissue shows an increased rigidity compared to the healthy state (CHAUDHURI et al., 2014; HUANG; INGBER, 2005). Higher acidity means that more acidic groups are saturated with protons which in turn impede the association of salt ions. As a result, ions are liberated and freely move within the electric field. It seems therefore reasonable to diagnose cancer by bioimpedance spectroscopy at the lowest possible frequency since there the differences between healthy and cancerous tissue are most distinct (HAEMMERICH et al., 2003, 2009; PRAKASH et al., 2015).

4.3 ACCESSING SKIN IMPEDANCE

The SC as the outermost layer provides a high resistance not only for drugs but also for electric current. A better contact can be made by using fluid gels or hydrogels, but this itself is again a possible error source due to shunt paths for the injected current (GRIMNES; MARTINSEN, 2015) . Other possibilities are soaking the skin with saline solution and stripping off the SC with tape, but this is a very time consuming procedure. Furthermore, the contact medium can have an influence as well (KESHTKAR et al., 2008; KHAN et al., 2016). Even if a good contact is made by a sufficient pressure application errors can arise because of

changing the internal structure of the tissue (DODDE; BULL; SHIH, 2012; GONZÁLEZ-CORREA et al., 2005; KESHTKAR; KESHTKAR, 2008). Another way to circumvent problems of dealing with little conductive surfaces is using invasive electrodes. That is also of advantage since otherwise only frequencies higher than 100 kHz are necessary to cover 90% of the viable skin in the case of a bipolar electrode (MARTINSEN; GRIMNES; HAUG, 1999). It can therefore be assumed that when the SC is passed, the measurement depth becomes independent upon frequency. Furthermore, the nonlinear effects that are caused by the activity of the sweat ducts (JOHNSEN et al., 2011) can also be circumvented.

Extensive clinical studies have been conducted with the Nevisense system (SciBase, Stockholm, Sweden) that uses microinvasive pins (MALVEHY et al., 2014; MOHR et al., 2013). The could diagnose BBC and SCC with a sensitivity of 98% and 100% whereas a sensitivity of 99.4% and 96.6% was reached in the first and second study, respectively, for the detection of malignant melanoma. The frequency range used lays between 1 Hz and 2500 kHz. At high frequency electrode effects can be avoided and their studies have shown the usability of impedance measurements by these types of electrodes.

However, the impedance of the skin is exclusively located in the SC (BIRGERSSON et al., 2013; GERSTNER, 1948; YAMAMOTO; YAMAMOTO, 1976). This means that when the SC is completely missing the remaining impedance is simply flat with almost no dispersion and has an extremely low value (GERSTNER, 1948; YAMAMOTO; YAMAMOTO, 1976). This makes it more difficult to distinguish between skin cancer and normal tissue. Moreover, most skin cancers are located directly underneath the SC. This means that even when the viable skin contributes little to the overall skin impedance at lower frequencies (MARTINSEN; GRIMNES; HAUG, 1999), skin cancer might already be detected. Good contact with the skin can also be made with conductive rubber since they are flexible (PENG et al., 2015b; ZHANG et al., 2016). This also decreases the influence of pressure application that even has an effect when using micro needle electrodes (RESNIK et al., 2015). Conductive rubber electrodes are already commercially available for the use of ECG recording, but for the use of skin impedance measurement there is little literature available. Only few studies dealt directly with this issue (KAUFMANN; ARDELT; RYSCHKA, 2013). Therefore, in the following chapter experiments will describe the carbon-based electrode probe used to measure the skin impedance.

5 EXPERIMENTS AND RESULTS

5.1 MICROELECTRODE FABRICATION

5.1.1 Paraffin wax with graphite

The principle of the electrode geometry resembles that used by Yamamoto, Yamamoto and Ozawa (1986). The central electrode was made from a tube of a 5 ml glass pipette which was broken at the upper end of the bulb. A wire of stainless steel was put into it and fixed with hot glue in the broken end. At the other end a mixture of paraffin wax with commercially available graphite was used.

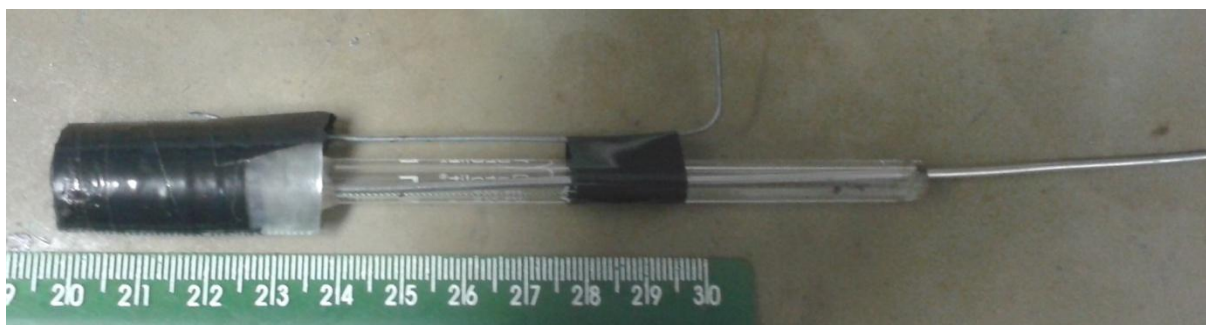
The paraffin wax and the graphite were put together in a small bowl and heated using a solder station until the wax was melted. The glass tube was then put on the molten mixture and let cooled. After that, more graphite was placed on the electrode tip and a heated metallic blade of a box cutter put on it so that more graphite could flow into the wax and raise the conductivity of the mixture.

For the outer electrode the lateral wall of a plastic pot was cut off. Therefrom a piece of 8 cm length was cut and rolled and taped with isolating tape so that a cylinder resulted with a diameter of 16 mm.

Again paraffin was mixed with graphite and the cylinder was put over the mixture let cooled. So that one end was filled with the mixture. After that, a hole was drilled with a hand drill. Through that hole the glass tube was put through.

A steel wire was put into the wax of the outer electrode. The wire was fixated with an isolating tape on the inner wall of the cylinder. The interspace between the outer cylinder and the glass tube was filled with foam plastic and pressed to the bottom in order to stabilize the glass tube.

Figure 11 - Side view of the electrode made from paraffin wax and graphite



Source: Author

5.1.2 Carbon fibers with silicone

For the production of the carbon paste electrode a glass test tube with a diameter of 18 mm was used for the outer electrode. Therefore, the bottom of the test tube was cut off in the following way. A cotton wick was wrapped around the tube approximately 12 cm away from the open end and soaked in ethanol. The wick was burned and right when the fire went out some water was dropped over it. A crack occurred and the bottom of the glass could be taken off. At the cut end some isolating tape was wrapped around in order to avoid lacerative.

The inner electrode was made from the tube of a 5 ml glass pipette. Again stainless steel rod was put into it and fixated with hot glue at one end. A bundle of carbon fibers was taken together and glued together by hand with silicone (CASCOLA, Henkel, Itapevi, SP).

This bundle was then inserted into the tube. In order to make sure that the whole opening is sealed, extremely short parts of the fibers were cut from the bundle and mixed with silicone (CASCOLA, Henkel, Itapevi, SP). With the tip of the blade of a box cutter the mixture was then smeared over the opening of the pipette.

The inner electrode was inserted into the test tube and pieces of nonheated hot glue were placed around it approximately 15 mm away from the lower end so that the inner electrode was more or less centered. A steel rod was placed at the inner wall of the outer tube and fixated with isolating tape at the upper end. The hot glue was heated with the heater of a solder station. The inner electrode placed in the center of the outer tube while the glue was hot and kept there while the glue was cooling. Simultaneously the steel rod was fixated at the wall.

A piece of aluminum paper was cut out according to the shape of the gap between the inner and the outer tube. On one side of the aluminum silicone (CASCOLA, Henkel, Itapevi,

SP) was smeared and pressed against a tissue of carbon fibers. The outer edge was cut out. Then on the surface of the cut out tissue silicone was again smeared and a new layer of carbon fiber tissue was pressed it. The outer edge was cut out again. This step was repeated a third time. Then the center hole was cut out. The space between the hot glue and the end of the tube was filled with aluminum paper. The layers of tissue were then placed on the top and at the outer edge silicone was distributed to seal the inner space.

Figure 12 – Cross section cut of the carbon fiber electrode: It shows the bundle of fibers in the central tube (1), the carbon fiber tissue of the outer electrode (2), the aluminum filling (3), the steel rods (4), the respective glass tubes for the electrodes (5) and the hot glue fixations (6).



Source: Author

Figure 13 - Top view of the electrode made of carbon fibers



Source: Author

Figure 14 - Side view of the electrode made of carbon fibers



Source: Author

5.2 CALIBRATION PROCEDURE OF THE ELECTRODE

In order to obtain the specific properties of the skin, it is necessary to determine the geometrical factor of the probe. This is done by a calibration procedure where the spectra of different concentrations of a saline solution are recorded. The calibration was done in two ways: experimental measurements; numerical simulation using FEMM. Since FEMM can only handle with axis-symmetric and plane problems, the geometric factor of the tetrapolar probe was only determined experimentally.

5.2.1 Experimental measurements

Starting with 200 mM NaCl solution, a dilution series was made by 3 steps down to 25 mM. The conductivity was measured with a conductivity meter (CD4303) at a temperature of 23°C. The equivalent impedance value was then calculated. In order to measure the impedance, a frequency sweep from 1 Hz to 1 MHz at 60 discrete frequencies was done with the HF2IS Impedance Spectroscope (Zurich Instruments, Zürich, CH). The impedance measurement of saline solutions was only done with the electrode that was made out of carbon fibers together with silicone, since the other model the measured values could not be reproduced. This was probably due to water infiltrating in the small gaps between the glass and the wax. The impedance values at approximately 37.7 kHz for concentrations of 200, 100, 50 and 25 mM were plotted against the correspondent conductivity. This frequency was used because here the phase angle was closest to 0°. The electrode was also short-circuited in order to know the resistance of the cables and the electrode material, which showed a resistance of 150 Ω. This value was subtracted from the impedance value. The final values are in table 1. Linear regression was used and the inclination was derived, then the cell constant was also calculated.

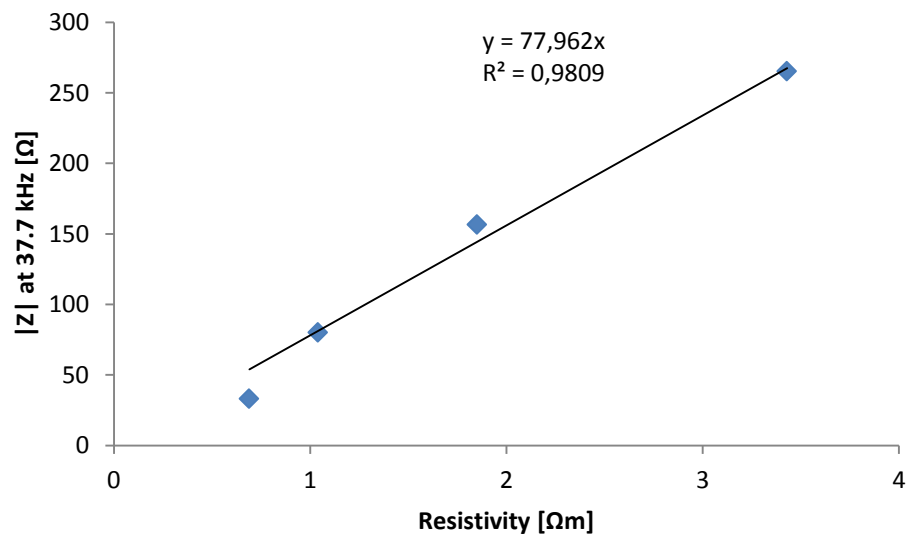
Table 1 - Measured values of the resistivity and the impedance of different saline solutions

| [NaCl] [mM] | Resistivity [Ωm] | Z at 37.7 kHz [Ω] |
|-------------|----------------------------------|-----------------------------|
| 200 | 0.69 | 33.1 |
| 100 | 1.04 | 80.0 |
| 50 | 1.85 | 157.6 |
| 25 | 3.43 | 265.3 |

Source: Author

The values of impedance were plotted against the resistivity using the Excel spreadsheet. The inclination of this trendline was calculated to be 77.96 m^{-1} with a coefficient of determination of 0.98.

Figure 15 - Impedance module at 37.7 kHz measured with the self made carbon fiber probe plotted against the resistivity of four different concentrations of saline solution



Source: Author

For the determination of the geometric factor of the tetrapolar probe the impedance values at 15. kHz were chosen since here the phase angle was close to 0° and plotted against the conductivity values measured with the conductivity meter. The measured values for the tetrapolar probe are shown in Table 2.

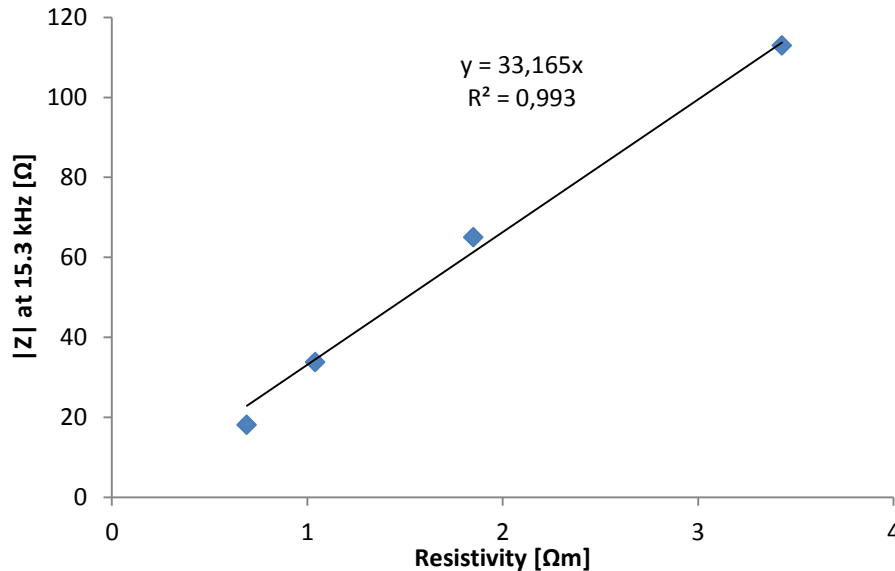
Table 2 - Measured values of the resistivity and the impedance of different saline solutions

| [NaCl] [mM] | Resistivity [Ωm] | Z at 15.3 kHz [Ω] |
|-------------|----------------------------------|-----------------------------|
| 200 | 0.69 | 18.14 |
| 100 | 1.04 | 33.8 |
| 50 | 1.85 | 64.98 |
| 25 | 3.43 | 112.79 |

Source: Author

By plotting these values against each other a value of 33.17 m^{-1} with coefficient of determination of 0.99 was determined (Figure 16).

Figure 16 - Impedance module at 15.3 kHz measured with the tetrapolar probe plotted against the resistivity of four different concentrations of saline solution



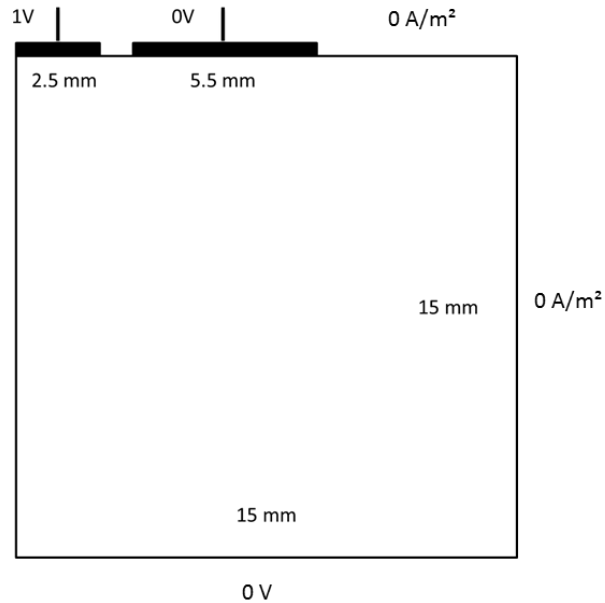
Source: Author

5.2.2 Numerical simulation

In FEMM a cylindrical tank with a radius and a height of 15 mm was indicated. The measures are shown in Figure 17. At the upper end a central conductor with a radius of 2.5 mm was placed. The voltage of this conductor was set to 1 V. Around this conductor lead another one with a width of 5.5 mm and 1 mm distant from the central conductor. The voltage of this conductor was set to 0 V. The bottom line of the tank was set to 0 V, too. The boundary condition of the other parts of the upper line that were not part of the conductors and the outer line were set to a current density of 0 A/m^2 . The values for the conductivity for a 200 mM, 100 mM, 50 mM and 25 mM NaCl solution were taken from the measurements with

the conductivity meter (CD4303). The permittivity values were taken from (PEYMAN; GABRIEL; GRANT, 2007) The mesh size was set by the program.

Figure 17 - Model and measures for the numerical simulation of saline solution measured with the home made probe



Source: Author

The resulting imaginary parts were in the $m\Omega$ range so that they can be regarded as negligible compared to the real ones. With the total current flowing over the center electrode the resistance could be calculated with Ohm's law (Equation 1). The resultant values of the resistance are shown in table 3.

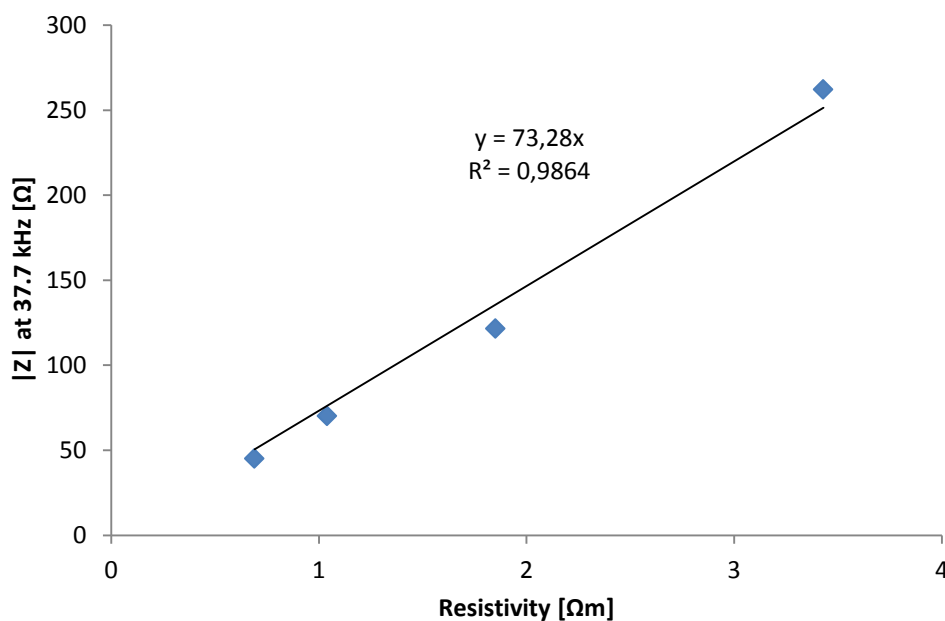
Table 3 - Measured resistivity and by simulation determined resistance values for different saline solutions

| [NaCl] [mM] | Resistivity [Ωm] | Resistance [Ω] |
|-------------|----------------------------|-------------------------|
| 200 | 0.69 | 45.0 |
| 100 | 1.04 | 70.0 |
| 50 | 1.85 | 121.4 |
| 25 | 3.43 | 262.0 |

Source: Author

Plotting these values against each other and generating a linear trendline with an intercept at the y-value 0 yielded an inclination of 73.28 m^{-1} with a coefficient of determination of 0.99.

Figure 18 - Calculated impedance values with FEMM plotted against the resistivities of four different concentrations of saline solution

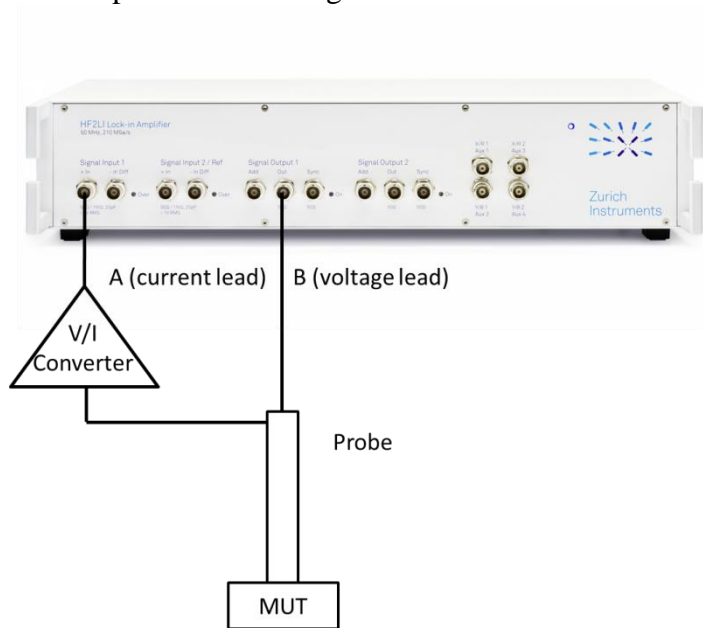


Source: Author

5.3 SKIN IMPEDANCE MEASUREMENT

The wires of the carbon electrode were connected by a crocodile clamp to both output (B) and signal input 1 (A) of a HF2IS Impedance Spectroscope (Zurich Instruments, Zürich, CH), respectively. In between the wire from the indifferent electrode and the signal input (A) a HF2TA Current Amplifier was linked. A voltage with amplitude of 1 V was applied in a frequency range between 1 Hz and 1 MHz in 60 discrete frequencies. 16 measurements at each discrete frequency were made and then averaging was calculated. The feedback resistance of the HF2TA was set to 1 k Ω .

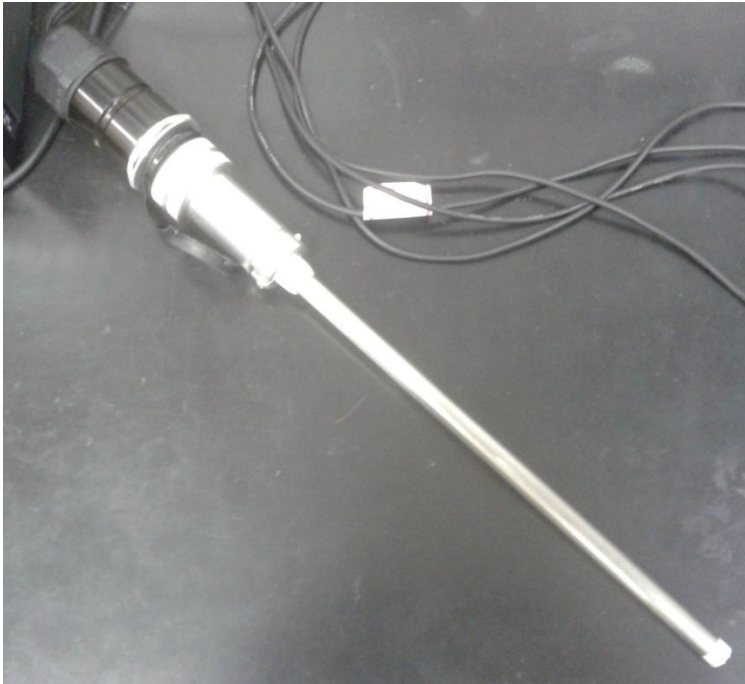
Figure 19 - Schematic of the experimental setting



Source: Author

For comparison measurements an in-house tetrapolar probe (Figure 20) was used. It consists of four hemispherical gold electrodes with a radius of 0.75 mm each. The electrodes are ordered so that two in line for the voltage application faced the other two on the opposite side. The interelectrode distance is 1 mm. Here the voltage pickup electrodes were connected to the signal input 2 of the HF2IS.

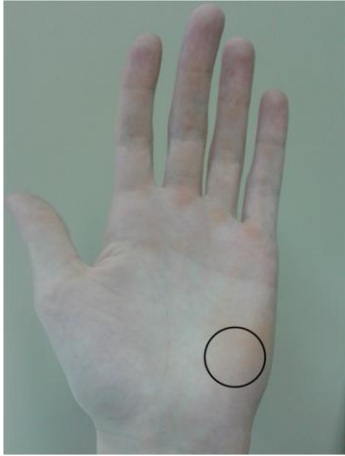
Figure 20 - Photograph of the tetrapolar probe used in this study



Source: Author

The measurements of the skin impedance were done over three consecutive days by following the same protocol. Five measuring sweeps were performed on each day. There was a time gap kept between the sweeps in order to leave the tissue recover itself and to avoid pressure artifacts. A second set of data was collected, but now the skin was wetted with a saline solution (0.9% NaCl). The measurements were done on the palm of the left hand (Fig. 17), as it is easy to access and makes a better electrode-skin contact. The skin was wetted by placing a saline droplet on the skin and smearing it after a few seconds.

Figure 21 - Measurement site



Source: Author

The measured module of the impedance, the phase, the resistance and reactance were recorded and saved in an Excel spreadsheet. In order to compare the results to those published in the literature, the results are presented in terms of complex relative permittivity and conductance. First, both real and imaginary parts of the permittivity were calculated according to equations (13) and (14). Second, those values were each divided by the electric field constant ϵ_0 . Finally, the module of the permittivity was finally calculated according to equation (3).

In order to fit the measured data, an iterative technique of the Excel solver was used for minimizing the sum of squared residuals. The experimental data were fitted into Cole elements (a resistor in series with another resistor parallel to a constant phase element). However, just one Cole element was used for fitting the measured spectra measured by the tetrapolar probe only one Cole element was necessary. The quality of the fit was calculated by using the relative root-mean-square deviation.

5.4 RESULTS

5.4.1 Impedance

5.4.1.1 Dry skin

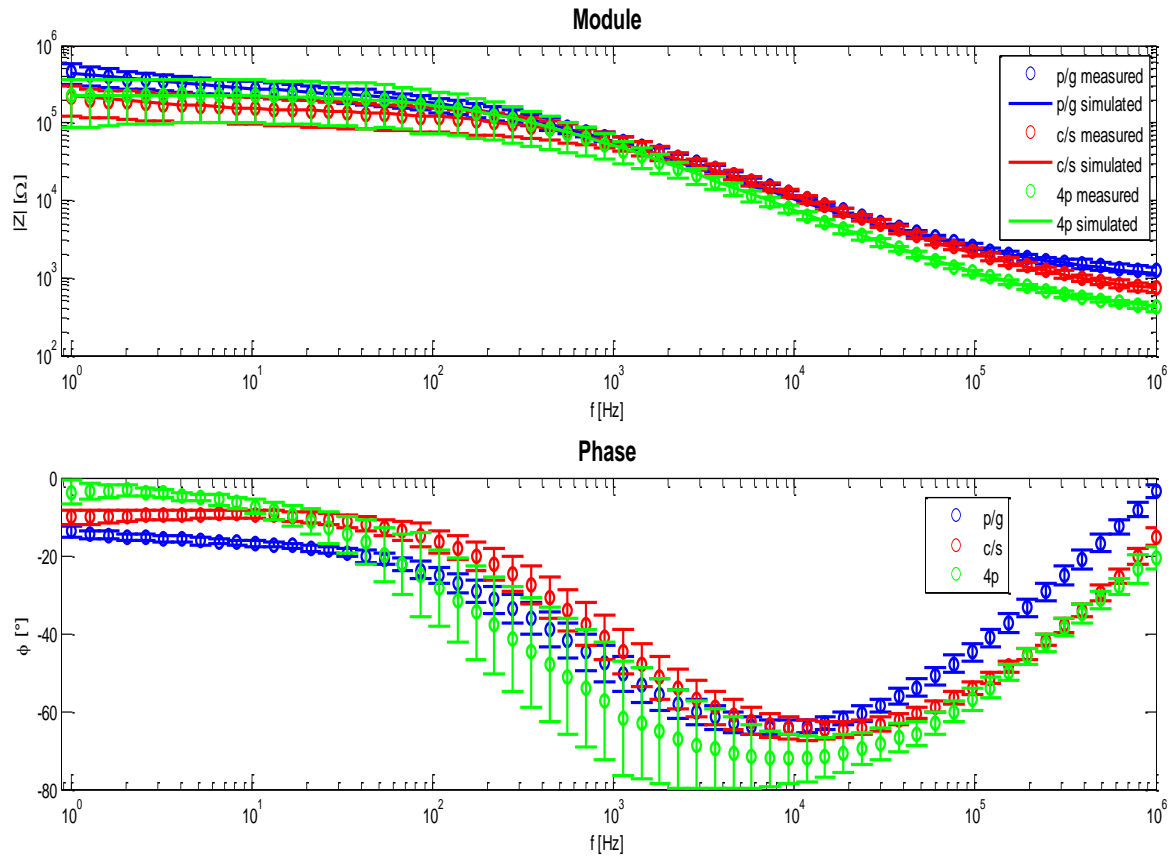
The spectrums of the impedance module are shown in figure 22. For the case of the probe made of paraffin wax and graphite (p/g) it can be observed that the impedance

decreases slowly from 455 k Ω to 160 k Ω until 100 Hz, and more rapidly to 1.27 k Ω at 1 MHz. The average error lies at 15.2%. A curve fit of the Cole parameters (see table 4) showed a root mean square deviation (RMSD) of 3.6%. It can also be observed that the phase angle remains relatively constant (20°) from 1 Hz to 100 Hz. The minimum phase of -65° was measured at 10 kHz and -3.4° at 1 MHz. The average phase error was approximately 7.6%.

The module of the measured impedance of the probe made of carbon fibers and silicone (c/s) was almost constant with a value of approximately 250 k Ω in the first frequency decade, the impedance, and then decreased to 760 Ω at 1 MHz. The maximum average error was 24%. The Cole fitting model showed a RMSD of 6.6%. The phase shift remains almost constant (= -10°) until 80 Hz, with a minimum of -68° at 10 kHz and reaches -20° at 1 MHz. The average error was 10.7%.

The impedance module measured with the tetrapolar probe (4p) remains relatively constant at a value of 23 k Ω from 1 Hz to 100 Hz and then falls down to a value of 475 Ω at 1 MHz. The average error is 33.5%. The values for the Cole fit can be seen in Table 4. The RMSD comprises 4.1%. The phase angle continually drops down from -3° to the minimum of -72.2° at 925 kHz and then rises up to -20.5° at 1 MHz. The average error here lies at 21.7%.

Figure 22 – Module (above) and phase (below) of dry palmar skin measured with a probe made of paraffin and graphite (p/g), of carbon fibers and silicone (c/s) and a tetrapolar probe (4p)



Source: Author

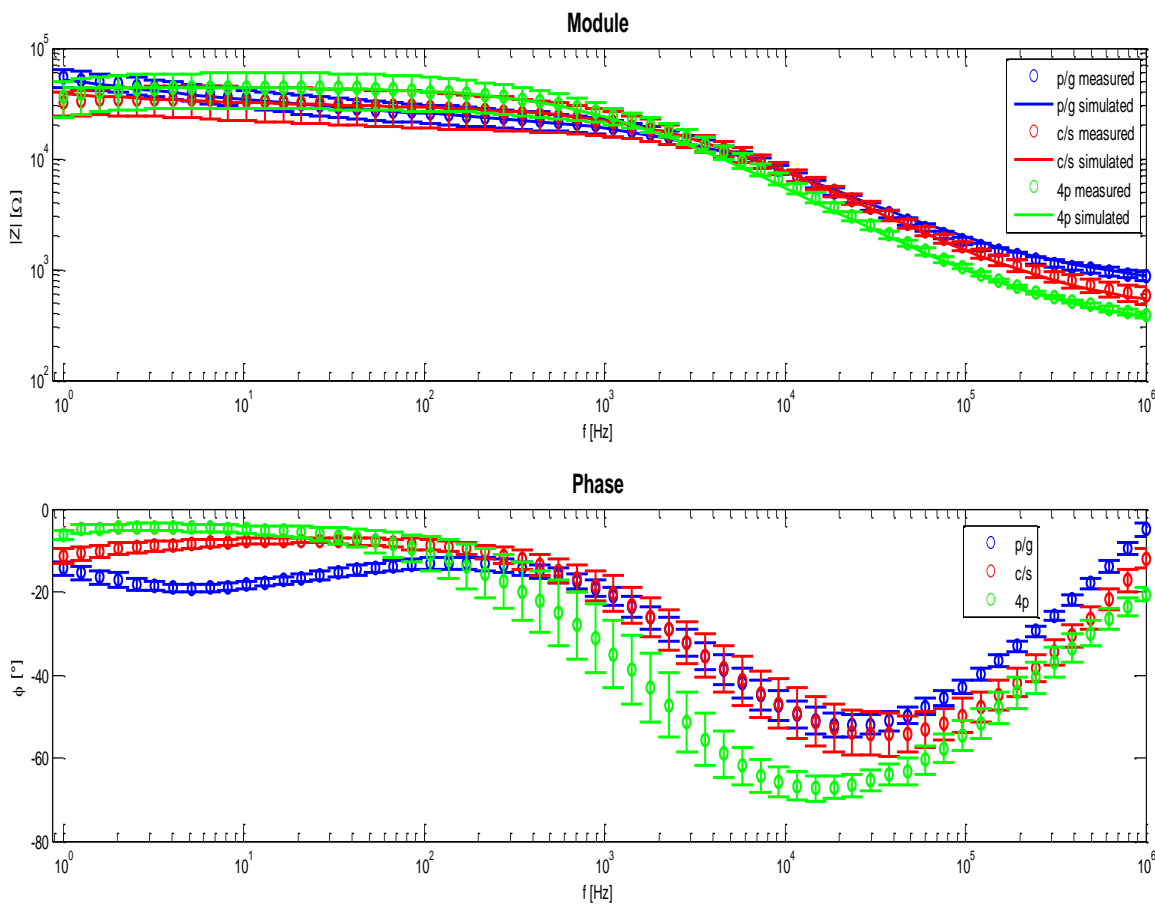
5.4.1.2 Wet skin

It can be seen in figure 23 that the measured impedance module measured with the p/g probe decreases from 54.2 to 25.6 k Ω at 1 to 100 Hz, respectively. At each frequency the wet skin impedance is smaller than the dry skin one. The average impedance error was 14.1%. A RMSD of 3.6% was also found for Cole model fitting. Contrary to the case of dry skin, the spectrum of the phase angle showed two minima. The first one at 5 Hz (-19 $^\circ$) and the second one (-52 $^\circ$) at 23.6 kHz. The average phase angle error was 8.1%.

The module of the skin impedance measured with the probe made of c/s, as shown in figure 23, is approximately 80 k Ω until 1 kHz and decreases to 650 Ω at 1 MHz. The RMSD of the measured values was 23.2% and 8.5% for the fitting error by the Cole equation. It can be seen that the phase angle increases from -15 $^\circ$ to -8 $^\circ$ from 1 to 50 Hz, respectively, has a minimum of -55 $^\circ$ at 37 kHz and was -10 $^\circ$ at 1 MHz. The RMSD was 12.7%.

The impedance module of the wet skin measured with probe 4p remains relatively stable at about 43.5 k Ω from 1 Hz to 100 Hz and then falls down to 428 Ω at 1 MHz. The average error is 20.9%. The values could be fitted to the Cole equation with a RMSD of 5%. The phase angle remains relatively stable at -5° from 1 Hz to 15 Hz. It then falls down to -67° at 15 kHz and then rises again up to -20° at 1 MHz. The average error of the phase angle comprises 18.2%.

Figure 23 - Module (above) and phase (below) of wet palmar skin measured with a probe made of paraffin and graphite (p/g), of carbon fibers and silicone (c/s) and a tetrapolar probe (4p)



Source: Author

5.4.2 Permittivity

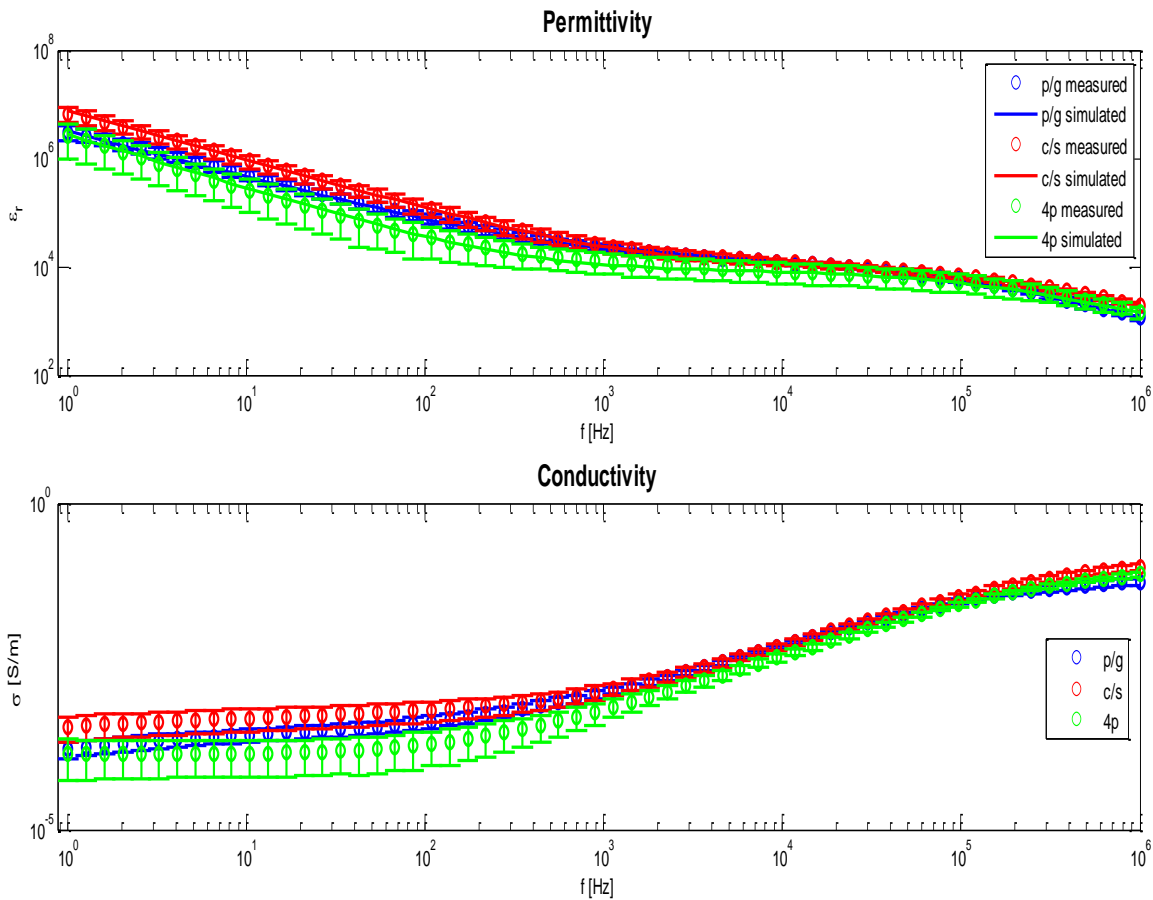
5.4.2.1 Dry skin

It can be seen in Figure 24 that the spectrum of the relative permittivity (ρ/g) shows two types of dispersions. The first dispersion appears between 1 Hz and 1 kHz, where the relative permittivity drops from 3,072,467 to 20,961. There is a small decrease from 1 to 100 kHz, but it decreases rapidly to 1,114 at 1 MHz. The average error of was 15.8%. The fitted Cole-Cole model used showed a RMSD of 7.5%. It can be noticed that the conductivity behaves in a reverse matter to the impedance module, increasing from 0.17 mS/m to 0.45 mS/m from 1 to 100 Hz. A conductivity of 61.2 mS/m was found at 1 MHz.

The relative permittivity measured with the probe c/s drops in the first three frequency decades from 6,611,437 to 22,797 and after a plateau down to 2,005 at 1 MHz. The average error was 21.1% and the Cole fitting model (table 4) showed a RMSD of 14.8%. The conductivity increases with increasing frequency at the first three decades (0.37 to 0.95 mS/m) and further to 123 mS/m at 1 MHz.

The relative permittivity falls sharply from 2,672,118 to 12 334 within the first three decades (4p). It then shows a broad step where it only falls relatively slightly down to 7.576 at 37.7 kHz followed by a second dispersion where it falls down to 1,443 at 1 MHz. The average error comprised 47%. The values could be fitted to the Cole-Cole equation with a RMSD of 20.4%. The conductivity remains almost constant around 0.15 mS/m from 1 Hz to 50 Hz and then rises sharply up to 80.4 mS/m at 1 MHz around which the inclination becomes weaker.

Figure 24 – Relative permittivity (above) and conductivity (below) of dry palmar skin measured with a probe made of paraffin and graphite (p/g), of carbon fibers and silicone (c/s) and a tetrapolar probe (4p)



Source: Author

5.4.2.2 Wet skin

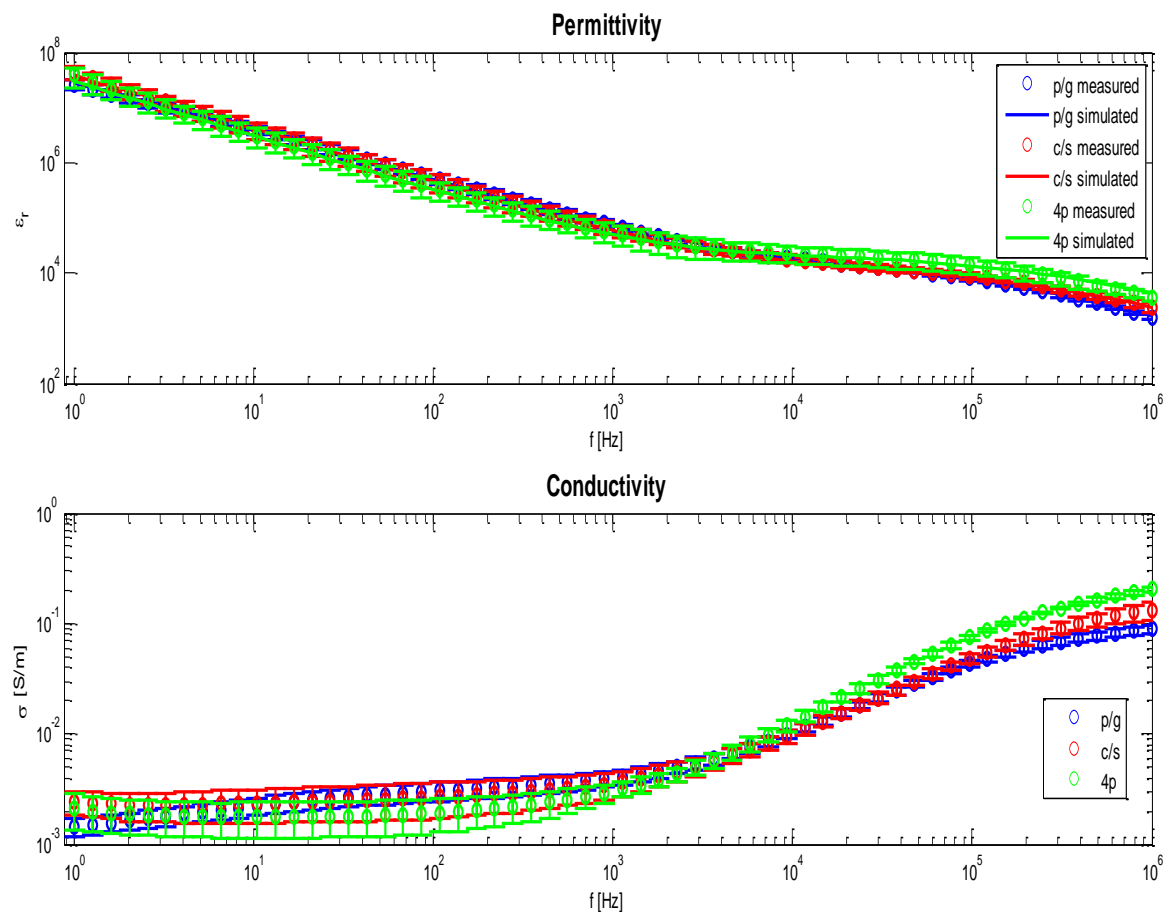
The relative permittivity (p/g) comprises a value of 38,053,952 at 1 Hz. It logarithmically falls down to about 30,876 at 4.6 kHz. It shows a step in between 10 and 100 kHz and falls down to 12600 at 1 MHz. The average error comprises 24%. A fit to the Cole-Cole equation with the values shown in table 5 could be achieved with a RMSD of 4.4%. The conductivity remains relatively constant between 2 and 3 mS/m between 1 and 500 Hz. It then increases in a sigmoidal shape up to 132.4 mS/m at 1 MHz.

With the probe c/s a value of 43,398,736 was measured at 1 Hz. It logarithmically falls down to 16,900 at 10 kHz, shows a step until about 100 kHz and falls further down to 2358 at 1 MHz. The average error comprises 23.9%. A fit to the Cole-Cole equation with the values shown in table 5 could be achieved with a RMSD of 10.7%. The conductivity remains

relatively constant between 2 and 3 mS/m between 1 and 500 Hz. It then increases in a sigmoidal shape up to 132.4 mS/m at 1 MHz.

The values measured with the probe 4p fall from 38,053,952 down to 37,679 in between 1 Hz and 1.8 kHz then the curve flattens a little bit and falls further down to 3656 at 1 MHz. The average error comprised 35%. The curve could be fitted to the Cole-Cole equation with the parameters listed in table 5 with a mean square root deviation of 10.8%. The conductivity remains relatively stable at 1.7 mS/m during the first two decades and then rises in a sigmoidal shape up to 0.2 S/m.

Figure 25 - Relative permittivity (above) and conductivity (below) of wet palmar skin measured with a probe made of paraffin and graphite (p/g), of carbon fibers and silicone (c/s) and a tetrapolar probe (4p)



Source: Author

5.4.3 Parameters of the fitting

Table 4 gives an overview of the parameters with whom the measured values of the impedance module were fitted. It was observed that that the wet skin impedance is 10 times

lower to the impedance of dry skin, especially at lower frequencies. It was also observed that R_{∞} decreases for wet skin, but also depends on the electrode type. For the electrode made out of paraffin wax and graphite (p/g) the impedance falls from 800 Ω to 500 Ω . For the one made out of carbon fibers it falls from 500 Ω to 400 Ω and in the case of the tetrapolar probe from 330 Ω to 290 Ω . The parameter α_h increases from 0.9 to 1 (p/g), from 0.86 to 0.94 (c/s) and from 0.93 to 0.9 (4p). What can also be seen is the fact that τ_h and ΔR_h decrease by a factor of ten when the skin is whetted. On the contrary, the time constant τ_1 of the second Cole element of the fitting for the p/g probe is with a value of 9214.61 s much higher when the skin is whetted than when the skin is dry with 2166.96 s. The same happens for ΔR_1 and α_1 . ΔR_1 changes from 18.8 M Ω to 807.9 k Ω and α_1 from 0.57 to 0.34.

Table 4 - Fitting parameters for the Cole equation for each type of electrode

| | p/g dry 4.1% | p/g wet 3.6% | c/s dry 6.6% | c/s wet 8.5% | 4p dry 3.1% | 4p wet 5% |
|---|-------------------------|-------------------------|-------------------------|-------------------------|------------------------|----------------------|
| R_{∞} [Ω] | 800 | 500 | 500 | 400 | 330 | 290 |
| ΔR_h [kΩ] | 215.1 | 18.7 | 133.5 | 28.6 | 230.7 | 43.7 |
| α_h | 0.9 | 1 | 0.86 | 0.94 | 0.93 | 0.9 |
| τ_h [ms] | 0.65 | 0.036 | 0.3 | 0.059 | 0.66 | 0.15 |
| ΔR_1 [kΩ] | 18,825.7 | 1,080.9 | 386,216 | 699.7 | | |
| α_1 | 0.5 | 0.4 | 0.6 | 0.48 | | |
| τ_1 [s] | 1,127.95 | 4,214 | 1.69 | 1,166 | | |

Source: Author

Table 5 shows all the parameters of the Cole-Cole fitting model to the measured data. Since the value for ϵ_{∞} could not be determined from the spectra over the given frequency range, it was voluntarily set to 80 which is the relative permittivity of water. Because of this the value for τ_h could not be determined accurately, as well as the values of $\Delta \epsilon_1$ and τ_1 . It can be observed that $\Delta \epsilon_h$ stays almost constant for the self made probes (p/g, c/s) when whetting the skin. Only with the tetrapolar probe with gold electrodes it increases from 8,073 up to 19,000. A significant change in the value of α_h as well as in the value of α_1 was not found.

Table 5 - Fitting parameters for the Cole-Cole equation for each type of electrode

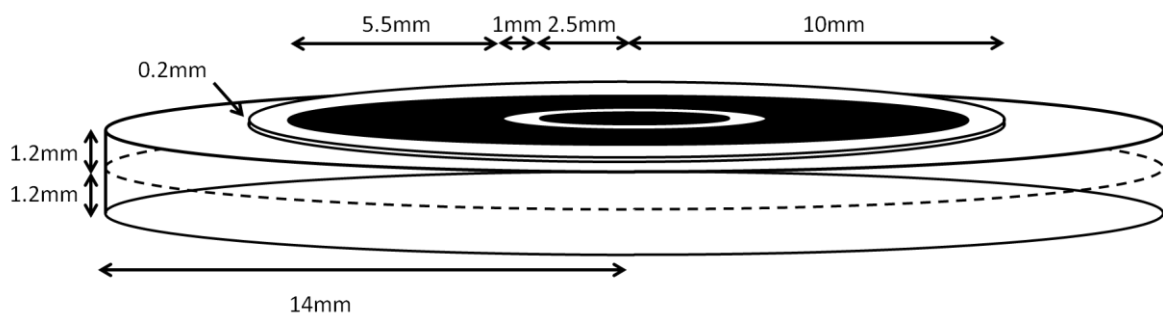
| | p/g dry 7.5% | p/g wet 11% | c/s dry 14.8% | c/s wet 4.4% | 4p dry 20.4% | 4p wet 14.3% |
|----------------------------------|-------------------------|------------------------|--------------------------|-------------------------|-------------------------|-------------------------|
| ϵ_{∞} | 80 | 80 | 80 | 80 | 80 | 80 |
| $\Delta\epsilon_h [\times 10^3]$ | 12.1 | 11.1 | 10.1 | 11.92 | 8.07 | 19 |
| α_h | 0.1 | 0.03 | 0.15 | 0.2 | 0.25 | 0.25 |
| $\tau_h [\mu s]$ | 2.33 | 1.12 | 1.08 | 1.1 | 1.6 | 1 |
| $\Delta\epsilon_l [\times 10^6]$ | 500 | 469 | 110 | 5000 | 110 | 1100 |
| α_l | 0.16 | 0.1 | 0.08 | 0.03 | 0 | 0 |
| $\tau_l [s]$ | 65.76 | 3.47 | 2.77 | 24.1 | 6.32 | 5.79 |

Source: Author

5.5 NUMERICAL SIMULATION OF THE SKIN IMPEDANCE WITH FEMM

A cylinder was defined with a radius of 14 mm and a depth of 2.4 mm. This cylinder was subdivided into two layers of 1.2 mm each which represent the viable skin (VS) and the subdermis (AT). On top of it a second cylinder was placed with a thickness of 200 μm , a value similar to the one measured for blister skin on the left hand palm by Martinsen, Grimnes and Sveen (1997). This one represented the SC. As boundary condition at the surface a current density of 0 A/m² was set. In order to decrease the processing time, the radius of this cylinder was set to 10 mm. At that distance away from the center the current densities was found to be negligible. The values for the sizes of the conductors were the same as in 5.2.2. The Potential of the central electrode was set to 1 V and the potential of the outer electrode to 0 V. The structure in total can be seen in figure 33.

Figure 26 - Dimensions of the skin model: The electrodes are shown in black



Source: Author

A simulation was done for the frequency of 100 Hz, 10 kHz and 1 MHz. For the mesh size for the SC a value of 10 μm was taken, for the other materials the program chose the mesh size. Finally the program created a mesh with 8876 nodes and 17038 elements. The values for the conductivity and the relative permittivity of the SC and the VS were chosen in a way that the final impedance values matched the measured ones with accuracy of at least 10%. The value of the loss tangent which is the phase shift in radian was taken by the measured values. The values for the AT were taken from Gabriel, Lau and Gabriel (1996). In absence of knowing the lateral and normal component of the conductivity and the relative permittivity of the tissue layers for both components the same values were taken. The parameters are listed in table 6.

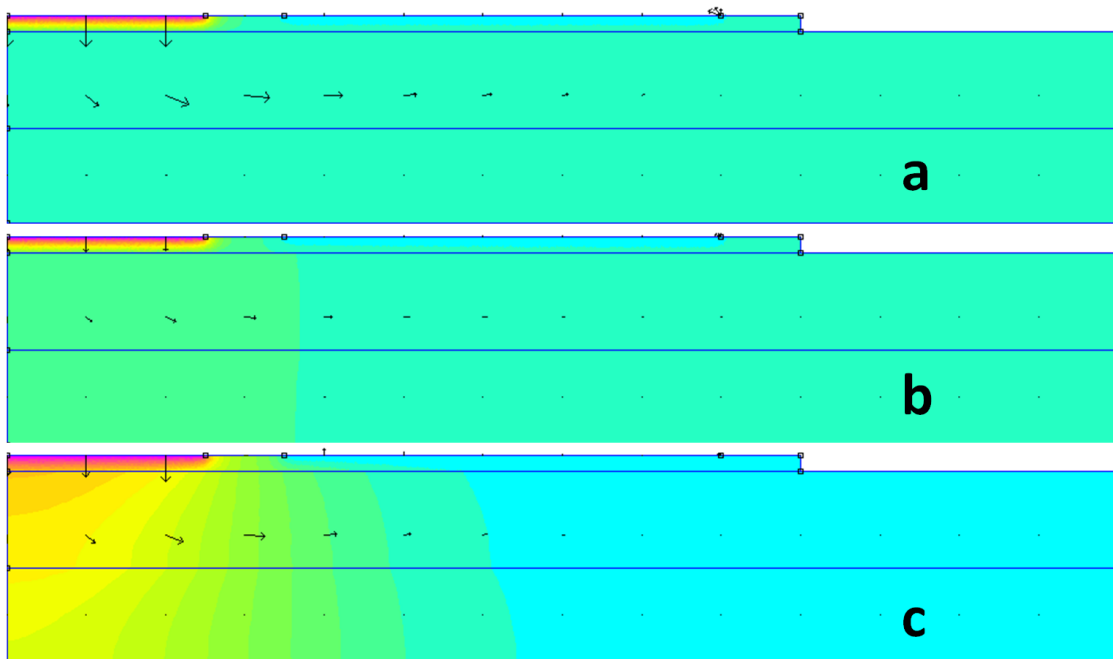
Table 6 - Material properties for the different layers of the skin model

| | | |
|---------------|-----------------------------------|--------------------------------|
| 100 Hz | σ [mS/m] | ϵ_r |
| SC | 0.085 | 5000 |
| VS | 200 | 400,000 |
| AT | 10 | 33,000 |
| 10 kHz | σ [mS/m] | ϵ_r |
| SC | 0.4 | 1700 |
| VS | 200 | 72,700 |
| AT | 10 | 1,000 |
| 1 MHz | σ [mS/m] | ϵ_r |
| SC | 25.5 | 60 |
| VS | 340 | 2900 |
| AT | 10 | 50 |

Source: Author

Figure 39 shows the potential distribution around the electrodes. The arrows indicate the strength of the real part of the current density with an amplification factor of 2.

Figure 27 - Potential distribution and current density lines in the skin model at 100 Hz (a), 10 kHz (b) and 1 MHz (c): The color violet indicates 1 V and the color light blue 0 V. Each color indicates an interval of 50 mV.



Source: Author

The values of the real (R) and imaginary (X) parts of the impedance for the three frequencies are listed in table 7.

Table 7 – Calculated real (R) and imaginary part (X) of the impedance of the skin model based on the values given in table 6

| Frequency | R | X |
|---------------|------------------|------------------|
| 100 Hz | 110.4 k Ω | -35.9 k Ω |
| 10 kHz | 4.6 k Ω | -9.5 k Ω |
| 1 MHz | 703.3 Ω | -188.5 Ω |

Source: Author

In order to determine the contribution of the VS to the overall impedance calculated in this simulation the real power of the VS was divided by the real power of the complete volume. The contribution of the VS to the complete impedance comprises 0.6% at 100 Hz, 14% at 10 kHz and 37.8% at 1 MHz.

6 DISCUSSIONS

6.1 DETERMINATION OF THE PROBE FACTOR

The value of the calculated geometric probe factor of 77.96 m^{-1} from measured data was close to 73.28 m^{-1} calculated by the FEMM simulation, which represents an error of 6.3%. According to equation (19) the value for a disc shaped electrode should be 63.6 m^{-1} and 100 m^{-1} for a hemispherical electrode according to equation (18). This means both experimental and numerical values lay between these analytical values from the equations. The conductivities of the solutions used were higher than 0.3 S/m while the highest conductivity measured on the skin was around 0.1 S/m . However, with the linear regression possible errors due to this discrepancy was minimized by the linear regression. The deviation between analytical and measured values found in the disc shaped electrode might be explained by the fact that the ions have a lower mobility in the proximity of the electrode surface. These results indicate a better usability for the homemade electrode. However, an experimental determination of the probe factor of the electrodes made of paraffin and graphite was not possible since the conductance was found to be dependent on time. One possible explanation might be leakage of solution into micro cracks or into the interspace between the glass tube and the wax.

6.2 SKIN IMPEDANCE MEASUREMENT

Reproducible results could be attained by the skin impedance measurements with the self made paraffin/graphite and carbon fiber/silicone electrode. The average error over the whole spectrum of the impedance module of dry skin comprised 15.2% and 24% for the paraffin/graphite and the carbon fiber electrode, respectively, in comparison to an average error of 33.5% with the tetrapolar probe. Less extreme was the difference in the case of wet skin. Here the average error lies at 14.1% and 23.2% compared to 20.9% error produced with the tetrapolar probe. While the errors for the self made electrodes are very similar the difference compared with the case of the tetrapolar probe is more than 10%. What caused this huge difference was the necessity to wet the skin a little bit in order to obtain a signal. With untreated skin no clear spectrum could be recorded.

A clear difference between the homemade electrodes and the tetrapolar probe was observed in the frequency range from 1 to 100 Hz, as any second dispersion was not observed

when using the tetrapolar probe. This dispersion below 10 Hz could be attributed to the effect of the electrode capacitance. The fittings to the Cole equations could in all cases be achieved with below a RMSD of 9%. The main derivation source was the form of the curve. Less accuracy of the modeling of wet skin was possible because up to 10 Hz influences from the instrumentation caused the real part of the impedance to increase, which in turn caused a derivation from the Cole behavior.

From the fitting process the values of α could be determined. They comprised values of 0.9 when the skin was dry and 1 when the skin was wet except for the tetrapolar probe where it remained at 0.9. These values are not in agreement with the literature data (BJÖRKLUND et al., 2013; KALIA; GUY, 1995; KONTTURI; MURATOMAKI, 1994), which report values around 0.7 and 0.8. It was also reported, that α decreases when the skin is whetted (YAMAMOTO; YAMAMOTO, 1977). A value close to 1 indicates that the material is very homogenous and shows a narrow distribution of relaxation times. When comparing the structure of the SC at the palms and other body parts (see figure 7 and 8) this should rather be true for the latter case. However in the presence of a lot of sweat ducts that provide straight current paths, they compensate for the greater inhomogeneity of palmar SC.

It could also be noted that the time constant τ_h decreased by a factor of 10 from the dry to the wet state. This is generally observed due to the fact that with higher moisturization the ions in the SC become more mobile and thereby reduce the value of ΔR_h which can be assumed to be the resistance of the SC (BJÖRKLUND et al., 2013).

The possibility that the lower impedance of wet skin was caused by the filling of sweat ducts during the preparation of the skin can be excluded for the following reason. It was shown that the filling of sweat ducts causes an increase in the skin conductance but does not influence the susceptance (MARTINSEN et al., 2015). In this study, however, the imaginary part of the impedance was affected by the wetting, so it can be assumed, that the higher hydration of the SC was the cause of the decrease of the impedance module (BJÖRKLUND et al., 2013; MARTINSEN; GRIMNES, 1998).

Whetting the skin had the effect to increase the time constant τ_1 from 2166.96 s to 9214.61 s in the measurements with the paraffin/graphite electrode. This seems to be parasitic effect due to the movement of ions either on the surface between measuring and indifferent electrode or due to movement of counterions against fixed charges within the SC.

The impedance of skin wetted with physiological solution was measured by (YAMAMOTO; YAMAMOTO; OZAWA, 1986) with an impedance probe similar to the self

made ones used in this study from 10 Hz to 10 MHz. The value at 10 Hz was 50 k Ω , which is in agreement with the values measured in this study at this frequency. The value then decreased over the whole frequency range while in this work it remains constant for one more decade and approached a constant value of some 100 Ω at 1 MHz. On dry skin the impedance spectrum in the work of (YAMAMOTO; YAMAMOTO; OZAWA, 1986) showed purely capacitive behavior as it could be seen on sites other than the palm of the hand in this study (data not shown).

It was reported that the capacitance of the SC increases by a factor of 1.5 (BJÖRKLUND et al., 2013). However, in this study the value of $\Delta\epsilon_h$ stays constant when the self-made probes were used. This could be explainable again by the presence of sweat ducts which provide a greater general humidity of the SC so that further moisturization has little effect.

Little differences could be observed for the impedances at high frequencies around 1 MHz. It is assumed that at these frequencies the influence of the VS becomes more dominant and that this skin layer is relatively unaffected by external treatment. The differences between the probe types are explainable with the different resistances of the electrodes themselves and in addition with a tetrapolar probe the influences of the cables can be avoided. Differences in between the different probe types are due to the different short circuit resistances. Including the resistances of the cables a value of about 330 Ω was found for the p/g probe and 150 Ω for the c/s probe. Subtracting these values from the overall impedance gives values close to the ones measured with the tetrapolar probe.

To sum up, it can be stated that the lower frequency limit is 10 Hz for the self-made probes work and that they can be used also until 1 MHz when the cable and electrode resistances are compensated for.

The conductivity of the dry skin below 1 kHz was between 0.17 to 0.45 mS/m, 0.37 to 0.95 mS/m and 0.15 mS/m for the three different probe types studied here. Gabriel et al. (1996) found a conductivity of 0.2 mS/m for dry skin. The measurements collected either by the self-made probes or by the tetrapolar probe were similar to the published one. On the contrary, the conductivities measured in this study increased with increasing frequency, while Gabriel, Lau and Gabriel (1996) found it not to be dependent on frequency.

In addition, Yamamoto and Yamamoto (1976) measured a conductivity of 10 μ S/m at 1 Hz, which is one order of magnitude lower than found in this study. Also Raicu, Kitagawa and Irimajiri (2000) measured a very low of conductivity increasing from 60 to 200 μ S/m within 0.1 to 1 kHz.

The high frequency values (1 MHz) of the conductivity are in all three cases by a factor of ten higher than the one determined by Gabriel, Lau and Gabriel (1996) which lies at 7 mS/m. The case is similar in comparison to the value measured by Yamamoto and Yamamoto (1976) who measured 14 mS/m. Good agreement could be achieved with the results of Raicu, Kitagawa and Irimajiri (2000).

Values for three discrete frequencies are shown in table 8 to give an overview of the measured and the literature data. To sum up, it can be stated that at low frequencies best agreement was with the work of Gabriel, Lau and Gabriel (1996) while at high frequencies best agreement was with Raicu, Kitagawa and Irimajiri (2000). Qualitatively, i.e. in regard of the shape of the curve, the measurements resemble the data of Yamamoto and Yamamoto (1976) best.

Table 8 – Experimental values from this study and literature values of conductivity at three different frequencies

| Conductivity [mS/m] | Yamamoto 1976 | Gabriel 1996 | Raicu 2000 | p/g | c/s | 4p |
|----------------------------|----------------------|---------------------|-------------------|------------|------------|-----------|
| 10 Hz | 0.01 | 0.2 | | 0.3 | 0.5 | 0.2 |
| 10 kHz | 0.1 | 0.2 | 1 | 7 | 6 | 5 |
| 1 MHz | 14 | 7 | 80 | 60 | 100 | 70 |

Source: GABRIEL; LAU; GABRIEL (1996); RAICU; KITAGAWA; IRIMAJIRI (2000); YAMAMOTO; YAMAMOTO (1976); Author

In terms of relative permittivity at low frequency, Gabriel, Lau and Gabriel (1996) found a constant value of 1,000 from 10 Hz up to 1 MHz. Yamamoto and Yamamoto (1976), however, measured an decreasing value of 10,000 at 1 Hz to 2,000 at 1 kHz. This value did not change notably until 100 kHz and then decreases down to 400 at 1 MHz. Raicu, Kitagawa and Irimajiri (2000) measured a relative permittivity of almost 20,000 at 100 MHz that decreased down to a value of 2,000 at 1 MHz.

In this study, the relative permittivity was between 2.5 and 8.79×10^5 for all electrode types at 10 Hz. This is a factor of about 400 higher compared to Gabriel, Lau and Gabriel (1996). At 1 MHz the values come closer together and the difference in between measured and literature data comprises a factor of about 6. The values for three frequencies are shown in table 9.

Table 9 – Experimental values from this study and literature values of relative permittivity at three different frequencies

| Permittivity | Yamamoto 1976 | Gabriel 1996 | Raicu 2000 | p/g | c/s | 4p |
|---------------|---------------|--------------|------------|--------------------|--------------------|--------------------|
| 10 Hz | 60,000 | 1,000 | | 4.44×10^5 | 8.79×10^5 | 2.52×10^5 |
| 10 kHz | 2,000 | 1,000 | 7,000 | 12,056 | 11,214 | 7,883 |
| 1 MHz | 400 | 1,000 | 2,000 | 1,121 | 1,872 | 1,436 |

Source: GABRIEL; LAU; GABRIEL (1996); RAICU; KITAGAWA; IRIMAJIRI (2000); YAMAMOTO; YAMAMOTO (1976); Author

The values for the conductivity of wet skin at frequencies below 1 kHz rises from 1.4 mS/m to 4.1 mS/m or stays around 2.5 and 1.7 mS/m for the paraffin electrode, the carbon fiber electrode and the tetrapolar probe, respectively. Gabriel, Lau and Gabriel (1996) measured the conductivity of wet skin with 0.3 mS/m at 10 Hz and 0.2 S/m at 1 MHz.

The differences compared with the literature data at 1 MHz could be due to cable resistances, other electrode geometries were used that cover more volume of the VS or due to the different measurement sites. At 10 kHz there was also good agreement with the work of Raicu, Kitagawa and Irimajiri (2000). The values for three frequencies of the literature and the ones measured in this study are listed in table 10 to give an overview.

Table 10 – Experimental values from this study and literature values of conductivity of wet skin at three different frequencies

| Conductivity [mS/m] | Gabriel 1996 | Raicu 2000 | p/g | c/s | 4p |
|---------------------|--------------|------------|-----|-----|-----|
| 10 Hz | 0.3 | | 2 | 2 | 2 |
| 10 kHz | 4 | 10 | 10 | 10 | 15 |
| 1 MHz | 200 | 300 | 90 | 130 | 190 |

Source: GABRIEL; LAU; GABRIEL (1996); RAICU; KITAGAWA; IRIMAJIRI (2000); Author

The relative permittivity of wet skin falls in all three cases from about 20×10^7 at 1 Hz down to 10,000 at around 20 kHz. The values then stay relatively constant for about two decades of frequency and the fall further down to 1,000 at 1 MHz.

In the work of Gabriel, Lau and Gabriel (1996) the relative permittivity shows a very weak first dispersion with an increment of 30,000 starting at a value of 63,000 at 10 Hz and a second dispersion with an increment of 30,000. The value at 1 MHz was about 3000 in their work. Compared to this study, the relative permittivity was 70 times higher at 10 Hz. Raicu, Kitagawa and Irimajiri (2000) measured a permittivity of about 100,000 at 100 Hz that decreased to 3000 at 1 MHz.

An overview of the values is given in table 11. At low frequencies the differences are enormous compared the values in the literature, as stated above. At higher frequencies the measured values in this study are by one third to one half lower than the literature data.

Table 11 – Experimental values from this study and literature values of permittivity of wet skin at three different frequencies

| Permittivity | Gabriel 1996 | Raicu 2000 | p/g | c/s | 4p |
|---------------------|---------------------|-------------------|--------------------|--------------------|--------------------|
| 10 Hz | 60,000 | | 3.83×10^6 | 4.98×10^6 | 3.05×10^6 |
| 10 kHz | 30,000 | 30,000 | 18,186 | 16,433 | 21,254 |
| 1 MHz | 3,000 | 3,000 | 1,680 | 2,358 | 4,395 |

Source: GABRIEL; LAU; GABRIEL, 1996; RAICU; KITAGAWA; IRIMAJIRI, 2000; Author

Compared to the literature data the permittivity and conductivity values in this study are much higher. However, the histological structure of the SC on the palms is different than at other anatomical sites (CHRISTOPHERS, 1971b; JANSEN, 1998). Moreover, at the palms there is a density of more than double of sweat ducts than on the forearm, where most impedance experiments are done (TAYLOR; MACHADO-MOREIRA, 2013; TRIPATHI et al., 2015). The sweat ducts can serve as an additional pathway of current and thereby explain the higher conductance at low frequencies (GRIMNES, 1983; PANESCU et al., 1993). Probably, that is why such enormous values of the relative permittivity were measured as seen in other tissue types (GABRIEL; LAU; GABRIEL, 1996).

6.3 SIMULATION OF SKIN IMPEDANCE

In table 11 the simulated values and the measured ones (dry skin, carbon fibers) for the real and imaginary parts of the skin impedance are shown. It can be seen that the values fit within a 5% error limit.

Table 12 - Real (R) and the imaginary (X) part of the impedance as measured on dry skin with the carbon fiber probe and calculated with a numerical simulation in FEMM. All values are given in Ω

| | R measured | R Simulation | X measured | X Simulation |
|---------------|-------------------|---------------------|-------------------|---------------------|
| 100 Hz | 109,000 | 110,400 | -35,600 | -35,898 |
| 10 kHz | 4,360 | 4,583 | -9,370 | -9,447 |
| 1 MHz | 701 | 703 | -188 | -188.5 |

Source: Author

In table 12 the conductivities for the different skin layers are listed as they are used in this work and by Huclova et al. (2011) and Birgersson et al. (2013) and as they were determined by Yamamoto and Yamamoto (1976). It can be observed that at 100 Hz and 10 kHz the conductivities are as four times higher than the ones determined by Yamamoto and Yamamoto (1976). The value at 1 MHz is almost as double as high. Since the conductance of the lead wires was not taken into account, the actual conductivity of the SC could be a little higher. As it was stated in 6.2, the conductivity of the skin at the palms could be higher (GRIMNES, 1983; PANESCU et al., 1993) because of the higher density of sweat ducts (TAYLOR; MACHADO-MOREIRA, 2013; TRIPATHI et al., 2015) in spite of it being much thicker. The values of the conductivity of the VS show good agreement with the values of Yamamoto and Yamamoto (1976). However, the values for the VS could not be determined with certainty in this study since its influence on the overall impedance was still very low at high frequencies.

In comparison to the calculated values by Birgersson et al. (2013) at 10 kHz the conductivity of the SC is 12 times higher and at 1 MHz five times higher. The conductivity of the VS is 100 mS/m higher at 10 kHz and three times as high at 1 MHz. However, the values of Birgersson et al. (2013) are based on an fitting of a five order polynomial which parameters are not directly correlated to the anatomy of the skin.

Huclova et al. (2011) did simulations in the microwave region. So only their values at 1 MHz shall be compared with the ones in this work. The SC has a conductivity of 188 mS/m which is about seven times higher. The conductivity of the VS is 160 mS/m higher than in this study. Huclova et al. (2011) used the experimental data of Naito, Hoshi and Yagihara (1998) to model the SC. In those studies the dielectric properties of SC powder was measured (NAITO; HOSHI; YAGIHARA, 1998) which could explain the differences.

Table 13 - Comparison of the conductivity values (in mS/m) of the SC and the VS used for this simulation study and in the literature

| 100 Hz | this work | Yamamoto | Birgersson | Huclova |
|---------------|------------------|-----------------|-------------------|----------------|
| SC | 0.085 | 0.02 | | |
| VS | 200 | 200 | | |
| 10 kHz | | | | |
| SC | 0.4 | 0.1 | 0.03 | |
| VS | 200 | 200 | 333 | |
| 1 MHz | | | | |
| SC | 25.5 | 14 | 5 | 188 |
| VS | 340 | 300 | 1000 | 500 |

Source: Author; BIRGERSSON et al., 2013; HUCLOVA et al., 2011; YAMAMOTO; YAMAMOTO, 1976

Also the values of the relative permittivity of the SC and the VS show close resemblance to the ones determined by Yamamoto and Yamamoto (1976) at 100 Hz and 10 kHz (table 13). At 1 MHz the relative permittivity of the SC is by more than a factor 10 smaller than in the work of Yamamoto and Yamamoto (1976) while the value for the VS is almost the same. This, again, could be due to the influence of the cables' conductance that was not taken into account in this study.

Again, a great deviation was found with the results of Birgersson et al. (2013) except for the relative permittivity of the SC at 1 MHz which matches the value received in this study perfectly. At 10 kHz the relative permittivity of the SC is about 6 times lower and the relative permittivity of the VS three times smaller than in this study and at 1 MHz about 15 times higher compared to Birgersson et al. (2013).

Huclova et al. (2011) used the dielectric properties of blood (GABRIEL; LAU; GABRIEL, 1996) to simulate the VS which shows the same relative permittivity as the VS (YAMAMOTO; YAMAMOTO, 1976). Like the conductivity, the value of the relative permittivity of the SC Huclova et al. (2011) used was is higher than in this study (this time by a factor 4). This again can be explained by the fact that SC powder was used to determine the relative permittivity of the SC (NAITO; HOSHI; YAGIHARA, 1998).

Table 14 - Comparison of the relative permittivity values of the SC and the VS used for this simulation study and in the literature

| 100 Hz | this work | Yamamoto | Birgersson | Huclova |
|---------------|------------------|-----------------|-------------------|----------------|
| SC | 5,000 | 3000 | | |
| VS | 400,000 | 400,000 | | |
| 10 kHz | | | | |
| SC | 1,700 | 1,500 | 300 | |
| VS | 100,000 | 100,000 | 300,000 | |
| 1 MHz | | | | |
| SC | 60 | 1000 | 60 | 240 |
| VS | 2900 | 3000 | 200 | 3000 |

Source: Author; BIRGERSSON et al., 2013; HUCLOVA et al., 2011; YAMAMOTO; YAMAMOTO, 1976

To sum up, at 100 Hz and 10 kHz the values of the relative permittivity of the SC and the VS determined by Yamamoto and Yamamoto (1976) could well be reproduced in this simulation study. Differences between the conductivity values of the SC can be explained by the different measurement sites, while the values for the VS show good agreement. However, the influence of the VS on the overall impedance was shown to be extremely small so that the

validity of the values for the VS should be taken with caution. At 1 MHz influences of the cables' conductance and of the VS become more prominent. This could explain the deviations from the literature data (YAMAMOTO; YAMAMOTO, 1976).

7 CONCLUSION AND PROPOSALS FOR FUTURE WORKS

7.1 CONCLUSION

Two types of impedance probes were fabricated for the recording of impedance spectra of human skin. The usage of carbon material allowed an easy and cheap fabrication and the geometry of two concentric surface electrodes avoided the occurrence of a complex electric field in the MUT. This study provided data of dielectric properties of skin below 100 Hz which is found seldom in the literature but important for estimating the effects of low frequency electromagnetic field exposure. This study showed that at the palm of the hand the conductivity of the skin is higher and the permittivity much higher than those given in the literature that were deduced from measurements on the forearm. A three layer skin model was simulated with the FEMM software, where the material specific properties of the three layers were adapted to the measured impedance values. The values of the dielectric properties used in the simulation study, however, showed good agreement with the literature data.

7.2 PROPOSALS FOR FUTURE WORKS

In order to reduce the measurement error at high frequencies and to avoid the effects of cable conductances, additional voltage measurements could be carried out. Furthermore, other electrode designs could be developed to improve the measurement depth of the probe. The electrode quality could be further improved by depositing active carbon or conductive polymers

In order to test the applicability of the probes developed in this work for example for diagnostic purposes sensitivity studies with physical skin phantoms in connection with the simulations of the skin model or with biological material less complex like potato could be done.

REFERENCES

- ABERG, P. et al. Non-invasive and microinvasive electrical impedance spectra of skin cancer - a comparison between two techniques. **Skin Research and Technology**, v. 11, n. 4, p. 281–6, 2005.
- ABIR, A. R.; RABBANI, K. S. Sensitivity study for a 4-electrode focused impedance method (FIM) using finite element method analysis. **Bangladesh Journal of Medical Physics**, v. 7, n. 1, p. 1–7, 2014.
- ABIR, R. et al. Effect of a spherical object in 4 electrode Focused Impedance Method (FIM): measurement and simulation. **Journal of Physics: Conference Series**, v. 434, n. 1, p. 12009, 18 abr. 2013.
- ACKER, H.; PIETRUSCHKA, F.; ZIEROLD, K. Comparative measurements of potassium and chloride with ion-sensitive microelectrodes and x-ray microanalysis in cultured skeletal muscle fibers. **In Vitro Cellular & Developmental Biology**, v. 21, n. 1, p. 45–48, jan. 1985.
- AGMON, N. et al. Protons and Hydroxide Ions in Aqueous Systems. **Chemical Reviews**, v. 116, n. 13, p. 7642–7672, 13 jul. 2016.
- AJETI, V. et al. Structural changes in mixed Col I/Col V collagen gels probed by SHG microscopy: implications for probing stromal alterations in human breast cancer. **Biomedical Optics Express**, v. 2, n. 8, p. 2307, 1 ago. 2011.
- AKBER, S. F. Water proton relaxation times of pathological tissues. **Physiological Chemistry and Physics and Medical NMR**, v. 40, p. 1–42, 2008.
- BARDELMEYER, G. H. Electrical conduction in hydrated collagen. I. Conductivity mechanisms. **Biopolymers**, v. 12, n. 10, p. 2289–2302, 1973.
- BERTEMES-FILHO, P. **Tissue Characterisation using an Impedance Spectroscopy Probe**. [s.l.] University of Sheffield, 2002.
- BERTEMES-FILHO, P. et al. Stand-off electrode (SoE): a new method for improving the sensitivity distribution of a tetrapolar probe. **Physiological Measurement**, v. 24, n. 2, p. 517–525, 1 maio 2003.
- BIRGERSSON, U. et al. Non-invasive bioimpedance of intact skin: mathematical modeling and experiments. **Physiological Measurement**, v. 32, n. 1, p. 1–18, 1 jan. 2011.
- BIRGERSSON, U. et al. A methodology for extracting the electrical properties of human skin. **Physiological Measurement**, v. 34, n. 6, p. 723–736, 2013.
- BJÖRKLUND, S. et al. Skin Membrane Electrical Impedance Properties under the Influence of a Varying Water Gradient. **Biophysical Journal**, v. 104, n. 12, p. 2639–2650, jun. 2013.

BORDI, F.; CAMETTI, C.; COLBY, R. H. Dielectric spectroscopy and conductivity of polyelectrolyte solutions. **Journal of Physics: Condensed Matter**, v. 16, n. 49, p. R1423–R1463, 2004.

BOTHWELL, T. P.; SCHWAN, H. P. Electrical Properties of the Plasma Membrane of Erythrocytes at Low Frequencies. **Nature**, v. 178, n. 4527, p. 265–266, 4 ago. 1956.

BOUWSTRA, J. A. et al. Structure of the skin barrier and its modulation by vesicular formulations. **Progress in Lipid Research**, v. 42, p. 1–36, 2003.

BROWN, B. H.; WILSON, A. J.; BERTEMES-FILHO, P. Bipolar and tetrapolar transfer impedance measurements from volume conductor. **Electronics Letters**, v. 36, n. 25, p. 2060, 2000.

BROWN, E. et al. Dynamic imaging of collagen and its modulation in tumors in vivo using second-harmonic generation. **Nature Medicine**, v. 9, n. 6, p. 796–801, 2003.

CARPENTER, D.; HOVEY, M. M.; BAK, A. F. Measurements of intracellular conductivity in Aplysia neurons: Evidence for organization of water and ions. **Annals of the New York Academy of Sciences**, v. 204, n. 1, p. 502–533, 1973.

CARPENTER, D. O.; HOVEY, M. M.; BAK, A. F. INTERNAL CONDUCTIVITY OF AXONS, NERVE CELL BODIES AND LARGE NONNERVOUS CELLS. v. AFRRI-SR75, n. March, 1975.

CHAUDHURI, O. et al. Extracellular matrix stiffness and composition jointly regulate the induction of malignant phenotypes in mammary epithelium. **Nature Materials**, v. 13, n. 10, p. 970–978, 2014.

CHEN, Y. et al. Poly(3,4-ethylenedioxythiophene) (PEDOT) as interface material for improving electrochemical performance of microneedles array-based dry electrode. **Sensors and Actuators, B: Chemical**, v. 188, p. 747–756, 2013.

CHRISTOPHERS, E. Die epidermale Columnärstruktur. **Zeitschrift für Zellforschung und Mikroskopische Anatomie**, v. 114, n. 3, p. 441–450, 1971a.

CHRISTOPHERS, E. Cellular Architecture of the Stratum Corneum. **Journal of Investigative Dermatology**, v. 56, n. 3, p. 165–169, mar. 1971b.

CLEGG, J. S. Properties and metabolism of the aqueous cytoplasm and its boundaries. **American Journal of Physiology-Regulatory, Integrative and Comparative Physiology**, v. 246, n. 2, p. R133–R151, fev. 1984.

COLE, K. S. PERMEABILITY AND IMPERMEABILITY OF CELL MEMBRANES FOR IONS. **Cold Spring Harbor Symposia on Quantitative Biology**, v. 8, n. 0, p. 110–122, 1940.

COLE, K. S.; COLE, R. H. Dispersion and Absorption in Dielectrics I. Alternating Current Characteristics. **The Journal of Chemical Physics**, v. 9, p. 341–351, 1941.

- CONWAY, B. E.; BIRSS, V.; WOJTOWICZ, J. The role and utilization of pseudocapacitance for energy storage by supercapacitors. **Journal of Power Sources**, v. 66, n. 1–2, p. 1–14, 1997.
- COPE, F. W.; DAMADIAN, R. Cell Potassium by ³⁹K Spin Echo Nuclear Magnetic Resonance. **Nature**, v. 228, n. 5266, p. 76–77, 3 out. 1970.
- DAMADIAN, R. Tumor Detection by Nuclear Magnetic Resonance. **Science**, v. 171, n. 3976, p. 1151–1153, 19 mar. 1971.
- DE SANTIS, V. et al. An equivalent skin conductivity model for low-frequency magnetic field dosimetry. **Biomedical Physics & Engineering Express**, v. 1, n. 1, p. 15201, 9 jun. 2015.
- DE SANTIS, V. et al. A novel homogenization procedure to model the skin layers in LF numerical dosimetry. **Physics in Medicine and Biology**, v. 61, n. 12, p. 4402–4411, 21 jun. 2016.
- DIAS, N. S. et al. New dry electrodes based on iridium oxide (IrO) for non-invasive biopotential recordings and stimulation. **Sensors and Actuators, A: Physical**, v. 164, n. 1–2, p. 28–34, 2010.
- DODDE, R. E.; BULL, J. L.; SHIH, A. J. Bioimpedance of soft tissue under compression. **Physiological Measurement**, v. 33, n. 6, p. 1095–1109, 1 jun. 2012.
- DONALDSON, P. J.; LEADER, J. P. Intracellular ionic activities in the EDL muscle of the mouse. **Pflügers Archiv European Journal of Physiology**, v. 400, n. 2, p. 166–170, 1984.
- EDELMANN, L. The physical state of potassium in frog skeletal muscle studied by ion-sensitive microelectrodes and by electron microscopy: interpretation of seemingly incompatible results. **Scanning microscopy**, v. 3, n. 4, p. 1219–30, 1989.
- EDMONDSON, R. et al. Three-Dimensional Cell Culture Systems and Their Applications in Drug Discovery and Cell-Based Biosensors. **ASSAY and Drug Development Technologies**, v. 12, n. 4, p. 207–218, maio 2014.
- EFTEKHARI, A.; LI, L.; YANG, Y. Polyaniline supercapacitors. **Journal of Power Sources**, v. 347, p. 86–107, abr. 2017.
- FOLETTI, M. C.; HAAS, S. E. Cutaneous melanoma: new advances in treatment. **Anais Brasileiros de Dermatologia**, v. 89, n. 2, p. 301–310, abr. 2014.
- FONG, C. N.; CHANG, D. C. K⁺-selective microelectrode study of internally dialyzed squid giant axons. **Biophysical Journal**, v. 53, n. 6, p. 893–897, jun. 1988.
- GABRIEL, S.; LAU, R. W.; GABRIEL, C. The dielectric properties of biological tissues: III. Parametric models for the dielectric spectrum of tissues. **Physics in Medicine and Biology**, v. 41, n. 11, p. 2271–2293, 1 nov. 1996.

GASCOYNE, P. R.; PETHIG, R.; SZENT-GYÖRGYI, A. Water structure-dependent charge transport in proteins. **Proceedings of the National Academy of Sciences of the United States of America**, v. 78, n. 1, p. 261–265, 1981.

GAUZA, M.; KUBISZ, L. Effect of water content on electrical conductivity of fish skin collagen. **Journal of Non-Crystalline Solids**, v. 357, n. 2, p. 686–690, jan. 2011.

GEDDES, L. A. Who introduced the tetrapolar method for measuring resistance and impedance? **IEEE Engineering in Medicine and Biology Magazine**, v. 15, n. 5, p. 133–134, 1996.

GERSTNER, H. Statistische Untersuchungen über den Wechselstromwiderstand der menschlichen Haut im Tonfrequenzgebiet. **Pflügers Archiv für die Gesamte Physiologie des Menschen und der Tiere**, v. 250, n. 1, p. 125–140, 1948.

GESELOWITZ, D. B. An application of electrocardiographic lead theory to impedance plethysmography. **IEEE transactions on bio-medical engineering**, v. 18, n. 1, p. 38–41, 1971.

GONZÁLEZ-CORREA, C. A et al. Electrical bioimpedance readings increase with higher pressure applied to the measuring probe. **Physiological Measurement**, v. 26, n. 2, p. S39–S47, 1 abr. 2005.

GRIMNES, S. Impedance measurement of individual skin surface electrodes. **Medical & Biological Engineering & Computing**, v. 21, n. 6, p. 750–755, nov. 1983.

GRIMNES, S.; MARTINSEN, Ø. G. Cole Electrical Impedance Model—A Critique and an Alternative. **IEEE Transactions on Biomedical Engineering**, v. 52, n. 1, p. 132–135, jan. 2005.

GRIMNES, S.; MARTINSEN, Ø. G. Sources of error in tetrapolar impedance measurements on biomaterials and other ionic conductors. **Journal of Physics D: Applied Physics**, v. 40, p. 9–14, 2006.

GRIMNES, S.; MARTINSEN, Ø. G. Electrodes. In: **Bioimpedance and Bioelectricity Basics**. 3. ed. Amsterdam: Elsevier, 2015. p. 179–254.

GULINO, M. et al. Role of water content in dielectric properties and delayed luminescence of bovine Achilles' tendon. **FEBS Letters**, v. 579, n. 27, p. 6101–6104, 2005.

HAEMMERICH, D. et al. In vivo electrical conductivity of hepatic tumours. **Physiological Measurement**, v. 24, n. 2, p. 251–260, 1 maio 2003.

HAEMMERICH, D. et al. Electrical conductivity measurement of excised human metastatic liver tumours before and after thermal ablation. **Physiological Measurement**, v. 30, n. 5, p. 459–466, 2009.

HINKE, J. A. Water and electrolyte content of the myofilament phase in the chemically skinned barnacle fiber. **The Journal of General Physiology**, v. 75, n. 5, p. 531–551, 1 maio 1980.

HINKE, J. A. M.; CAILLÉ, J. P.; GAYTON, D. C. Distribution and State of Monovalent Ions in Skeletal Muscle Based on Ion Electrode, Isotope, and Diffusion Analyses. **Annals of the New York Academy of Sciences**, v. 204, n. 1, p. 274–296, 1973.

HUANG, S.; INGBER, D. E. Cell tension, matrix mechanics, and cancer development. **Cancer Cell**, v. 8, n. 3, p. 175–176, 2005.

HUCLOVA, S. et al. Sensitivity and specificity analysis of fringing-field dielectric spectroscopy applied to a multi-layer system modelling the human skin. **Physics in Medicine and Biology**, v. 56, n. 24, p. 7777–7793, 21 dez. 2011.

JANSEN, T. Bedeutung und Funktion des Stratum corneum. **Deutsches Ärzteblatt**, v. 95, n. 6, p. A-284, 1998.

JOHNSEN, G. K. et al. Memristive model of electro-osmosis in skin. **Physical Review E**, v. 83, n. 3, p. 31916, 24 mar. 2011.

JOHNSEN, G. K. An introduction to the memristor - a valuable circuit element in bioelectricity and bioimpedance. **Journal of Electrical Bioimpedance**, v. 3, n. 1, p. 20–28, 2012.

JONSCHER, A. K. The Interpretation of Non-Ideal Dielectric Admittance and Impedance Diagrams. **Physica Status Solidi (a)**, v. 32, n. 2, p. 665–676, 16 dez. 1975.

JONSCHER, A. K. The “universal” dielectric response. **Nature**, v. 267, n. 5613, p. 673–679, 23 jun. 1977.

KALIA, Y. N.; GUY, R. H. The Electrical Characteristics of Human Skin in Vivo. **Pharmaceutical Research**, v. 12, n. 11, p. 1605–1613, 1995.

KATO, Y. et al. Acidic extracellular microenvironment and cancer. **Cancer Cell International**, v. 13, n. 1, p. 89, 2013.

KAUFMANN, S.; ARDELT, G.; RYSCHKA, M. Measurements of Electrode Skin Impedances using Carbon Rubber Electrodes – First Results. **Journal of Physics: Conference Series**, v. 434, n. 1, p. 12020, 18 abr. 2013.

KESHTKAR, A. et al. Surface fluids effects on the bladder tissue characterisation using electrical impedance spectroscopy. **Medical Engineering and Physics**, v. 30, n. 6, p. 693–699, 2008.

KESHTKAR, A.; KESHTKAR, A. The effect of applied pressure on the electrical impedance of the bladder tissue using small and large probes. **Journal of Medical Engineering & Technology**, v. 32, n. 6, p. 505–511, 2008.

KESHTKAR, A.; KESHTKAR, A.; SMALLWOOD, R. H. Electrical impedance spectroscopy and the diagnosis of bladder pathology. **Physiological measurement**, v. 27, n. 7, p. 585–596, 2006.

- KHAN, S. et al. Prostate Cancer Detection Using Composite Impedance Metric. **IEEE Transactions on Medical Imaging**, v. 35, n. 12, p. 2513–2523, dez. 2016.
- KONTTURI, K.; MURTOMAKI, L. Impedance Spectroscopy in Human Skin: A Refined Model. **Pharmaceutical Research**, v. 11, n. 9, p. 1355, 1994.
- KUNZE, D. L.; BROWN, A. M. Internal Potassium and Chloride Activities and the Effects of Acetylcholine on Identifiable Aplysia Neurones. **Nature New Biology**, v. 229, n. 8, p. 229–231, 24 fev. 1971.
- KURZWEIL-SEGEV, Y. et al. Dielectric Relaxation of Hydration Water in Native Collagen Fibrils. **The Journal of Physical Chemistry B**, v. 121, n. 21, p. 5340–5346, 23 jun. 2017.
- LACY, K.; ALWAN, W. Skin cancer. **Medicine**, v. 41, n. 7, p. 402–405, jul. 2013.
- LEE, C. O. Activities of potassium and sodium ions in rabbit heart muscle. **The Journal of General Physiology**, v. 65, n. 6, p. 695–708, 1 jun. 1975.
- LEI, K. F.; WU, Z.-M.; HUANG, C.-H. Impedimetric quantification of the formation process and the chemosensitivity of cancer cell colonies suspended in 3D environment. **Biosensors and Bioelectronics**, v. 74, p. 878–885, 15 dez. 2015.
- LIN, S.-J. et al. Discrimination of basal cell carcinoma from normal dermal stroma by quantitative multiphoton imaging. **Optics Letters**, v. 31, n. 18, p. 2756, 15 set. 2006.
- LING, G. N. The Physical State of K⁺ and Na⁺ in Living Cells. In: **In Search of the Physical Basis of Life**. Boston, MA: Springer US, 1984. p. 227–269.
- LING, G.; WALTON, C. What retains water in living cells? **Science**, v. 191, n. 4224, p. 293–295, 23 jan. 1976.
- MALLEO, D. et al. Note: Characterization of electrode materials for dielectric spectroscopy. **Review of Scientific Instruments**, v. 81, n. 1, p. 16104, jan. 2010.
- MALVEHY, J. et al. Clinical performance of the Nevisense system in cutaneous melanoma detection: An international, multicentre, prospective and blinded clinical trial on efficacy and safety. **British Journal of Dermatology**, v. 171, n. 5, p. 1099–1107, 2014.
- MARTINSEN, Ø. G. et al. Sources of error in AC measurement of skin conductance. **Journal of Electrical Bioimpedance**, v. 6, n. 1, p. 49, 29 dez. 2015.
- MARTINSEN, Ø. G.; GRIMNES, S. On using single frequency electrical measurements for skin hydration assessment. **Innovation et technologie en biologie et médecine**, v. 19, n. 5, p. 395–399, 1998.
- MARTINSEN, Ø. G.; GRIMNES, S.; SVEEN, O. Dielectric properties of some keratinised tissues. Part 1: Stratum corneum and nail in situ. **Medical & Biological Engineering & Computing**, v. 35, n. 3, p. 172–176, maio 1997.

- MARTINSEN, Ø. S. G.; GRIMNES, S.; HAUG, E. Measuring depth depends on frequency in electrical skin impedance measurements. **Skin Research and Technology**, v. 5, n. 3, p. 179–181, ago. 1999.
- MAUGHAN, D.; RECCHIA, C. Diffusible sodium, potassium, magnesium, calcium and phosphorus in frog skeletal muscle. **The Journal of Physiology**, v. 368, n. 1, p. 545–563, 1 nov. 1985.
- MOHR, P. et al. Electrical impedance spectroscopy as a potential adjunct diagnostic tool for cutaneous melanoma. **Skin Research and Technology**, v. 19, n. 2, p. 75–83, 2013.
- MOUW, J. K.; OU, G.; WEAVER, V. M. Extracellular matrix assembly: a multiscale deconstruction. **Nature Reviews Molecular Cell Biology**, v. 15, n. 12, p. 771–785, 5 dez. 2014.
- NAITO, S.; HOSHI, M.; YAGIHARA, S. Microwave dielectric analysis of human stratum corneum in vivo. **Biochimica et Biophysica Acta (BBA) - General Subjects**, v. 1381, n. 3, p. 293–304, ago. 1998.
- NEWMAN, J. Resistance for Flow of Current to a Disk. **Journal of The Electrochemical Society**, v. 113, n. 5, p. 501, 1966.
- NOURI, K. **Skin Cancer**. Columbus: McGraw-Hill, 2008.
- ORDINARIO, D. D. et al. Bulk protonic conductivity in a cephalopod structural protein. **Nature Chemistry**, v. 6, n. 7, p. 596–602, 2014.
- PANESCU, P. et al. The mosaic electrical characteristics of the skin. **IEEE Transactions on Biomedical Engineering**, v. 40, n. 5, p. 434–439, maio 1993.
- PASTUSHENKO, I. et al. Squamous Cell Carcinomas of the Skin Explore Angiogenesis-Independent Mechanisms of Tumour Vascularization. **Journal of Skin Cancer**, v. 2014, p. 1–5, 2014.
- PAULY, H. Über die elektrische Kapazität der Zellmembran und die Leitfähigkeit des Zytoplasmas von Ehrlich-Aszitestumorzellen. **Biophysik**, v. 1, n. 3, p. 143–153, set. 1963.
- PAULY, H. Über den physikalisch-chemischen Zustand des Wassers und der Elektrolyte in der lebenden Zelle. **Biophysik**, v. 10, n. 1, p. 7–32, mar. 1973.
- PENG, H.-L. et al. Flexible dry electrode based on carbon nanotube/polymer hybrid micropillars for biopotential recording. **Sensors and Actuators A: Physical**, v. 235, n. Supplement C, p. 48–56, nov. 2015a.
- PENG, H.-L. et al. Flexible dry electrode based on carbon nanotube/polymer hybrid micropillars for biopotential recording. **Sensors and Actuators A: Physical**, v. 235, n. Supplement C, p. 48–56, nov. 2015b.
- PETHIG, R. Dielectric studies of proton transport in proteins. **Ferroelectrics**, v. 86, p. 31–39, 1988.

PETHIG, R.; KELL, D. B. The passive electrical properties of biological systems: their significance in physiology, biophysics and biotechnology. **Physics in Medicine and Biology**, v. 32, n. 8, p. 933–970, 1 ago. 1987.

PEYMAN, A.; GABRIEL, C.; GRANT, E. H. Complex permittivity of sodium chloride solutions at microwave frequencies. **Bioelectromagnetics**, v. 28, n. 4, p. 264–274, maio 2007.

PLIQUETT, U. et al. Testing miniaturized electrodes for impedance measurements within the beta-dispersion – a practical approach. **Journal of Electrical Bioimpedance**, v. 1, n. 1, p. 41, 2010.

PLIQUETT, U. Bioimpedance: A Review for Food Processing. **Food Engineering Reviews**, v. 2, n. 2, p. 74–94, jun. 2010.

POLLACK, G. H.; CAMERON, I. L.; WHEATLEY, D. N. **Water and the Cell**. Dordrecht: Springer Netherlands, 2006.

PRAKASH, S. et al. Ex vivo electrical impedance measurements on excised hepatic tissue from human patients with metastatic colorectal cancer. **Physiological Measurement**, v. 36, n. 2, p. 315–328, 1 fev. 2015.

RABBANI, K. S. et al. Focused impedance measurement (FIM): A new technique with improved zone localization. **Annals of the New York Academy of Sciences**, v. 873, p. 408–420, 1999.

RABBANI, K. S.; KARAL, M. A. S. A new four-electrode Focused Impedance Measurement (FIM) system for physiological study. **Annals of Biomedical Engineering**, v. 36, n. 6, p. 1072–1077, 2008.

RAICU, V.; KITAGAWA, N.; IRIMAJIRI, A. A quantitative approach to the dielectric properties of the skin. **Physics in Medicine and Biology**, v. 45, n. 2, p. L1–L4, 1 fev. 2000.

REBOIRAS, M. D.; PFISTER, H.; PAULY, H. Activity coefficients of salts in highly concentrated protein solutions. **Biophysical Chemistry**, v. 9, n. 1, p. 37–46, nov. 1978.

RESNIK, D. et al. Characterization of skin penetration efficacy by Au-coated Si microneedle array electrode. **Sensors and Actuators A: Physical**, v. 232, p. 299–309, 2015.

ROFSTAD, E. K. et al. Acidic extracellular pH promotes experimental metastasis of human melanoma cells in athymic nude mice. **Cancer Research**, v. 66, n. 13, p. 6699–6707, 2006.

SALTER, D. C. **Describing relaxing systems which evolve with time**. Conference on Electrical Insulation & Dielectric Phenomena - Annual Report 1978. **Anais...**Pocono Manor, PA: IEEE, out. 1978

SALTER, D. C. **Studies in the measurement, form and interpretation of some electrical properties of normal and pathological human skin in vivo**. [s.l.] University of Oxford, 1981.

SASAKI, N. Dielectric properties of slightly hydrated collagen: Time-water content superposition analysis. **Biopolymers**, v. 23, n. 9, p. 1725–1734, set. 1984.

SCHMID, G.; CECIL, S.; ÜBERBACHER, R. The role of skin conductivity in a low frequency exposure assessment for peripheral nerve tissue according to the ICNIRP 2010 guidelines. **Physics in Medicine and Biology**, v. 58, n. 13, p. 4703–4716, 2013.

SCHMID, G.; HIRTL, R. On the importance of body posture and skin modelling with respect to in situ electric field strengths in magnetic field exposure scenarios. **Physics in Medicine and Biology**, v. 61, n. 12, p. 4412–4437, 21 jun. 2016.

SCHWAN, H. P. et al. On the low-frequency dielectric dispersion of colloidal particles in electrolyte solution. **The Journal of Physical Chemistry**, v. 66, n. 12, p. 2626–2635, dez. 1962.

SRINIVASARAGHAVAN, V. et al. A comparative study of nano-scale coatings on gold electrodes for bioimpedance studies of breast cancer cells. **Biomedical Microdevices**, v. 16, n. 5, p. 689–696, 28 out. 2014.

TAYLOR, N. A.; MACHADO-MOREIRA, C. A. Regional variations in transepidermal water loss, eccrine sweat gland density, sweat secretion rates and electrolyte composition in resting and exercising humans. **Extreme Physiology & Medicine**, v. 2, n. 1, p. 4, 2013.

TOMASELLI, V. P.; SHAMOS, M. H. Electrical properties of hydrated collagen. II. Semiconductor properties. **Biopolymers**, v. 13, n. 12, p. 2423–2434, dez. 1974.

TRIPATHI, S. R. et al. Morphology of human sweat ducts observed by optical coherence tomography and their frequency of resonance in the terahertz frequency region. **Scientific Reports**, v. 5, n. 1, p. 9071, 13 ago. 2015.

WOLF, M. et al. Broadband dielectric spectroscopy on human blood. **BBA - General Subjects**, v. 1810, n. 8, p. 727–740, 2011.

WOLF, M. et al. Relaxation dynamics of a protein solution investigated by dielectric spectroscopy. **Biochimica et Biophysica Acta**, v. 1824, n. 5, p. 723–730, 2012.

WU, X. et al. Sodium Dodecyl Sulfate doping PEDOT to enhance the performance of neural microelectrode. **Journal of Electroanalytical Chemistry**, v. 758, p. 26–32, 1 dez. 2015.

YA-XIAN, Z.; SUETAKE, T.; TAGAMI, H. Number of cell layers of the stratum corneum in normal skin - relationship to the anatomical location on the body, age, sex and physical parameters. **Archives of Dermatological Research**, v. 291, n. 10, p. 555–559, 8 nov. 1999.

YAMAMOTO, T.; YAMAMOTO, Y. Electrical properties of the epidermal stratum corneum. **Medical & Biological Engineering**, v. 14, n. 2, p. 151–158, mar. 1976.

YAMAMOTO, T.; YAMAMOTO, Y. Analysis for the change of skin impedance. **Medical and Biological Engineering and Computing**, v. 15, n. 3, p. 219–227, 1977.

YAMAMOTO, Y.; YAMAMOTO, T.; OZAWA, T. Characteristics of skin admittance for dry electrodes and the measurement of skin moisturisation. **Medical & biological engineering & computing**, v. 24, n. 1, p. 71–77, 1986.

YAO, S.; ZHU, Y. Nanomaterial-Enabled Dry Electrodes for Electrophysiological Sensing: A Review. **JOM**, v. 68, n. 4, p. 1145–1155, 3 abr. 2016.

ZHANG, H. et al. A Motion Interference-Insensitive Flexible Dry Electrode. **IEEE Transactions on Biomedical Engineering**, v. 63, n. 6, p. 1136–1144, jun. 2016.

ZHENG, J. Energy metabolism of cancer: Glycolysis versus oxidative phosphorylation (review). **Oncology Letters**, v. 4, n. 6, p. 1151–1157, 2012.

APPENDIX A: Technical specifications of the probes of this study compared to literature

| | p/g | c/s | Gabriel et al. (1996) | Raicu et al. (2000) |
|--|-----------------------|-----------------------|-------------------------------|----------------------------|
| Short circuit resistance | 230 Ω | 50 Ω | 50 Ω (including cable) | not known |
| Inner electrode radius | 2,5 mm | 2,5 mm | not known | 1.75 mm |
| inner radius of counter electrode | 3,5 mm | 3,5 mm | not known | 2.25 mm |
| outer radius of counter electrode | 9 mm | 9 mm | not known | not known |
| geometric factor | 77.96 m^{-1} | 77.96 m^{-1} | not known | 208 m^{-1} |
| frequency range | 1 Hz-1 MHz | 1 Hz-1 MHz | 10 Hz-20 GHz | 100 Hz-100 MHz |

APPENDIX B: Protocol of the FEMM modeling for the skin impedance at 1 MHz

```
[Format] = 1
[Precision] = 1e-008
[Frequency] = 1000000
[MinAngle] = 30
[Depth] = 1
[LengthUnits] = millimeters
[ProblemType] = axisymmetric
[Coordinates] = cartesian
[Comment] = "Add comments here."
[PointProps] = 0
[BdryProps] = 2
<BeginBdry>
  <BdryName> = "New Boundary"
  <BdryType> = 2
  <vsr> = 0
  <vsi> = 0
  <qsr> = 0
  <qsi> = 0
  <c0r> = 0
  <c0i> = 0
  <c1r> = 0
  <c1i> = 0
<EndBdry>
<BeginBdry>
  <BdryName> = "bottom"
  <BdryType> = 2
  <vsr> = 0
  <vsi> = 0
  <qsr> = 0
  <qsi> = 0
  <c0r> = 0
```

```
<c0i> = 0
<c1r> = 0
<c1i> = 0
<EndBdry>
[BlockProps] = 3
<BeginBlock>
  <BlockName> = "VS"
  <ox> = 0.34000000000000002
  <oy> = 0.34000000000000002
  <ex> = 2900
  <ey> = 2900
  <ltx> = 0
  <lty> = 0
<EndBlock>
<BeginBlock>
  <BlockName> = "AT"
  <ox> = 0.01
  <oy> = 0.01
  <ex> = 50
  <ey> = 50
  <ltx> = 0
  <lty> = 0
<EndBlock>
<BeginBlock>
  <BlockName> = "SC"
  <ox> = 0.025499999999999998
  <oy> = 0.025499999999999998
  <ex> = 65
  <ey> = 65
  <ltx> = 0
  <lty> = 0
<EndBlock>
[ConductorProps] = 2
<BeginConductor>
```

```

<ConductorName> = "electrode sensing"
<vcr> = 1
<vci> = 0
<qcr> = 0
<qci> = 0
<ConductorType> = 1
<EndConductor>
<BeginConductor>
<ConductorName> = "electrode indifferent"
<vcr> = 0
<vci> = 0
<qcr> = 0
<qci> = 0
<ConductorType> = 1
<EndConductor>
[NumPoints] = 12
2.5  0    0    0    0
3.5  0    0    0    0
9    0    0    0    0
10   0    0    0    0
14   -2.6140000000000003  0  0  0
10   -0.19900000000000001  0  0  0
14   -1.4139999999999999  0  0  0
0    0    0    0    0
0    -0.19900000000000001  0  0  0
0    -1.4139999999999999  0  0  0
0    -2.6140000000000003  0  0  0
14   -0.20000000000000001  0  0  0
[NumSegments] = 14
3    5    -1    2    0    0    0
2    3    -1    2    0    0    0
1    2    -1    0    0    0    2
4    6    -1    2    0    0    0

```

| | | | | | | |
|----|----|----|---|---|---|---|
| 7 | 0 | -1 | 0 | 0 | 0 | 1 |
| 8 | 5 | -1 | 0 | 0 | 0 | 0 |
| 9 | 6 | -1 | 0 | 0 | 0 | 0 |
| 10 | 4 | -1 | 2 | 0 | 0 | 0 |
| 10 | 9 | -1 | 0 | 0 | 0 | 0 |
| 9 | 8 | -1 | 0 | 0 | 0 | 0 |
| 8 | 7 | -1 | 0 | 0 | 0 | 0 |
| 5 | 11 | -1 | 2 | 0 | 0 | 0 |
| 11 | 6 | -1 | 2 | 0 | 0 | 0 |
| 0 | 1 | -1 | 2 | 0 | 0 | 0 |

[NumArcSegments] = 0

[NumHoles] = 0

[NumBlockLabels] = 3

| | | | | | |
|--------------------|-----------------------|---|------|---|---|
| 2.5105 | -0.062100000000000002 | 3 | 0.02 | 0 | 0 |
| 2.71 | -0.82999999999999996 | 1 | -1 | 0 | 0 |
| 2.9399999999999999 | -1.6699999999999999 | 2 | -1 | 0 | 0 |